The interaction between endogenous GABA, functional connectivity and behavioral flexibility is critically altered with advanced age

Kirstin-Friederike Heise[1,2*], Laura Rueda-Delgado[1,3], Sima Chalavi[1,2], Bradley R. King[1,2,4], Thiago Santos Monteiro[1,2], Richard A. E. Edden[5,6], Dante Mantini[1,7], Stephan P. Swinnen[1,2]

[1] Department of Movement Sciences, Movement Control and Neuroplasticity Research Group, KU Leuven

[2] KU Leuven Brain Institute, Leuven, Belgium

[3] School of Psychology, Trinity College Dublin, Dublin 2, Ireland

[4] Department of Health & Kinesiology, College of Health, University of Utah, Salt Lake City, Utah, USA

[5] The Russell H. Morgan Department of Radiology and Radiological Science, The Johns Hopkins University School of Medicine, Baltimore, MD, USA

[6] F. M. Kirby Research Center for Functional Brain Imaging, Kennedy Krieger Institute, Baltimore, MD, USA

[7] Brain Imaging and Neural Dynamics Research Group, IRCCS San Camillo Hospital, Venice, Italy

[*]Correspondence to
Kirstin-Friederike Heise
Movement Control and Neuroplasticity Research Group
KU Leuven
Tervuurse Vest 101; 3001 Leuven, Belgium
Email: kirstin.heise@kuleuven.be

Abstract

The flexible adjustment of ongoing behavior challenges the nervous system's dynamic control mechanisms and has shown to be specifically susceptible to age-related decline. Previous work links endogenous gamma-aminobutyric acid (GABA) with behavioral efficiency across perceptual and cognitive domains, with potentially the strongest impact on those behaviors that require a high level of dynamic control. Based on the integrated analyses of behavior and modulation of interhemispheric phase-based connectivity during dynamic motor state transitions and endogenous GABA concentration, we provide converging evidence for age-related differences in the behaviorally more beneficial state of endogenous GABA concentration. We suggest that the increased interhemispheric connectivity seen in the older adults represents a compensatory mechanism caused by rhythmic entrainment of neural populations in homotopic motor cortices. This mechanism appears to be most relevant in the presence of a less optimal tuning of the inhibitory tone to uphold the required flexibility of behavioral action.

Abbreviations

AP, anti-phase; DV, dependent variable; EEG, electroencephalography; GABA, γ-aminobutyric acid; GLMM, generalized linear mixed effects model; IP, in-phase; ISPC, inter-site phase clustering; IV, independent variable; MRS, magnetic resonance spectroscopy; M1, primary motor cortex; NAA, N-acetylaspartate; OCC, occipital cortex; SNR, signal-to-noise ratio.

Introduction

Flexibly adjusting ongoing behavior poses a specific challenge to the neural control mechanisms and this becomes particularly visible with increasing age [1]. Functional deficits in endogenous γ-aminobutyric acid (GABA)-mediated neural signaling represent one suspect mechanism among the many potential causes of age-related behavioral decline [2]. GABAergic interneurons are suggested to have a major role in scaling and fine-tuning neural oscillations [reviewed in [3,4]]. More specifically, GABAergic neurotransmission is believed to be an essential regulator of phase synchronization of neural oscillations [reviewed in [5]], which has been proposed to constitute one of the brain's main modes of communication [6,7]. Thus, phase-based connectivity is indicative of the time-sensitive modulation of inter-site neural communication and therefore serves as a proxy for the responsiveness of the neural system.

Previous work indicates that GABAergic synaptic mechanisms on the cortical level, evaluated at resting-state, predict the system's capacity for dynamic event-related modulation of cortical inhibition, and that this is linked to efficient motor control [8]. This work suggests that, once baseline GABAergic neurotransmission is imbalanced, the system's responsiveness is impaired and this may have detrimental behavioral consequences. Such imbalance may occur at older age when disinhibition becomes more prominent. Experimental evidence for this association between age-related GABAergic dysfunction and declining behavior across perceptual and cognitive domains points towards a stronger impact on those types of behavior that require a high level of dynamic control [e.g. [9–11]]. Yet, lowered motor cortical GABA levels are found to correlate with age-related changes in sensorimotor connectivity and diminished motor control [12]. These recent findings suggest a broader link between GABA availability and connectivity as a read-out for neural communication with implications for behavioral efficiency. However, whether these phenomena are simply co-occurring or whether they can be attributed to underlying causal mechanisms still remains an open question.

Here, we chose a behavioral paradigm involving the dynamic control of transitions between dynamical motor states of varying complexity, which has shown to engage widespread, and in particular interhemispheric, neural communication within the sensorimotor system [13,14]. Our main

interest was to shed light on the nature of the interactions between task-related connectivity dynamics, behavior, and tuning of the motor-cortical inhibitory system in the course of healthy aging. Therefore, we employed a multimodal approach to fuse endogenous GABA levels with the dynamic modulation of interhemispheric motor-cortical phase synchronization in the context of motor-state transitions in neurotypical young and older volunteers.

Results

To investigate the impact of individual variations in baseline GABA levels for the association between interhemispheric motor-cortical connectivity and complex bimanual behavior, we used a cross-sectional multimodal approach. The participants underwent in total three sessions, including magnetic resonance spectroscopy (MRS) in the first session and the second session to familiarize themselves with the behavioral paradigm (motor state transitions). The third session followed 24 hours after the familiarization and involved electroencephalography (EEG) during task performance. MRS data were used to extract the endogenous GABA concentration. EEG data served to compute the task-related functional connectivity metric based on the circular variance of frequency-specific phase angle differences alongside the behavioral parameters (Figure 1, see Materials and Methods section for details). While the unimodal analyses (neurochemical, neural, behavioral) served to verify expected age-differences, our primary interest was to integrate all three modalities to investigate the character of their interactions.

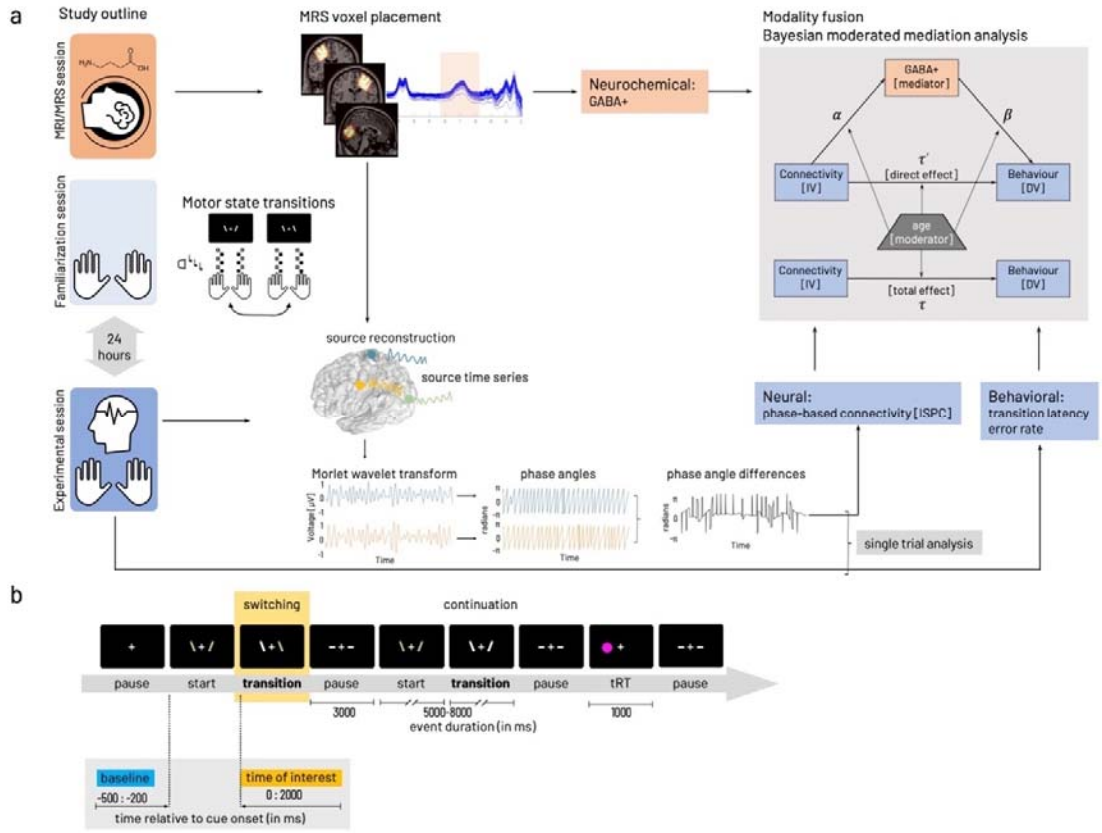

Figure 1: Experimental procedures and parameters of interest. a) Study outline *with MRI/MRS (session 1), task familiarization (session 2) preceding the main experiment (session 3) including EEG during task performance. Edited MRS and T1-weighted images were used to extract tissue-corrected GABA levels and additional macromolecules (GABA+) from left and right primary motor and occipital voxels. The behavioral paradigm involved transitions between a stable (mirror-symmetric in-phase tapping, left) and a less stable (anti-phase tapping, right) motor state. Task familiarization included stimulus-response mapping and individual performance frequency adjustment. Performance in motor state transitions was described with transition latency and error rate. The EEG signal was projected into source space based on the centroid coordinates of the GABA voxels. Phase angles were computed based on spectrally decomposed (Morlet wavelet transform) source time series. Phase angle differences between source signal pairs were used to compute connectivity (inter-site phase clustering, ISPC) between cortical sources. Phase angle differences were associated with behavioral performance in a single trial-based analysis. Then parameters of interest from the individual modalities (neurochemical, neural, behavioral) were integrated with a Bayesian moderated mediation analysis estimated for interhemispheric motor-cortical connectivity as independent variable [IV]. In both cases, dependent variable [DV] behavior was either median transition latency or cumulative error rate. Details on formalization of model paths $\alpha, \beta, \tau', \tau$ given in Methods.* ***b) Flow of events within the behavioral paradigm.*** *Phases of finger movement ('start', 'continuation', 'switching') were interleaved with rest phases ('pause'). A randomly occurring reaction time task ('tRT'), a fast key press with either left or right thumb in response to appearance of a circle on the side of the required response was interspersed with the other events with a 5% probability of occurrence. Inlay highlights the time zones relevant for the analysis of behavioral data and EEG/EMG data analysis (time of interest, yellow). Data collected in the within-trial pause (demarked in blue) was used as baseline for the EEG/EMG analysis of the data from the time of interest (yellow). A high-resolution version of this figure can be accessed under https://figshare.com/s/aae99a05f0fab30304f2*

GABA+ concentration

To examine the endogenous motor-cortical GABA concentration, MRS data from left, right primary motor cortex (M1), and a control region, i.e. the occipital cortex (OCC) were acquired in 22 older and 22 young adults. In two cases (one older, one young), the data of the right M1 were excluded from

further analysis due to motion artifacts and insufficient model fit. Consistency of the voxel placement across participants and individual traces of edited spectra for each voxel were visually inspected (Figure 2). Quantitative quality metrics were comparable to those published in recent studies from our and other groups [15–17] (for descriptive statistics see Supplementary Table 1).

A gamma generalized linear mixed model (GLMM, identity link) was fitted to predict GABA+ with GROUP (young, older) and VOXEL (left M1, right M1, OCC) as factors of interest. All quality metrics (see Methods for details) and raw grey matter fraction (GM fraction) were added as covariates (after mean-centering) to identify their influence on GABA+ levels and their potential interaction with voxel or group through stepwise backward selection. This procedure revealed that of all quality metrics only GABA Fit error interacted with voxel and raw GM fraction interacted with group (Supplementary Table 2), all other interactions (all p>.2) were excluded from the final model. Of note, only interactions were removed during backward selection but all factors and covariates were kept in the final model to control for their influence. The final model (Supplementary Table 3) confirmed a significant effect of GABA signal-to-noise ratio (GABA SNR, Type II Wald $X^2(1) = 6.74$, $p < .01$) and Frequency offset (Type II Wald $X^2(1) = 17.20$, $p < .0001$). Additionally, compared to the occipital voxel, both sensorimotor voxels tended to show higher GABA+ levels with increasing GABA Fit Error (VOXEL × GABA Fit Error (centered), Type II Wald $X^2(2) = 5.84$, $p = .05$). Relative to the young, the older showed overall lower GABA+ levels with increasing GM fraction (β = -0.49±0.19, 95%CI [-0.86, -0.12], X^2=-2.61, $p < .01$, GROUP × raw GM fraction (centered), Type II Wald $X^2(1) = 6.82$, $p < .01$, Figure 2d) across all voxels.

With reference categories young and occipital voxel, we found an overall average GABA+ level around 2.86 i.u. (intercept $\beta = 2.86 \pm 0.26$, 95% CI [2.34, 3.37], $X^2 = 10.8$, $p < .0001$). Based on the Type II Wald statistics, GABA+ was found to be significantly different between age groups and this was specific to the voxel (GROUP × VOXEL $X^2(2) = 9.57$, $p < .01$, Figure 2c). Specifically, marginal means contrast estimated for the individual parameter levels of the GROUP × VOXEL interaction revealed lower GABA+ levels in both sensorimotor voxels compared to the occipital voxel in the older (OCC-LM1: ΔEMM=1.65±0.227, 95%CI [0.99, 2.32], z=7.29, $p_{holm} < .0001$; OCC-RM1:

143 ΔEMM=1.564±0.2, 95%CI [0.93, 2.20], z=7.27, p_{holm} <.0001) while the young showed no differences
144 between the voxels (marginal means contrasts given in Supplementary Table 4). Furthermore, the
145 older showed significantly lower GABA+ levels in both sensorimotor voxels compared to the young
146 (LM1: ΔEMM=0.64±0.15, 95%CI [0.21, 1.07], z=4.40, p_{holm} <.0001; RM1: ΔEMM=0.55±0.12,
147 95%CI [0.19, 0.91], z=4.48, p_{holm} <.0001) but not the occipital voxel.
148 In short, controlling for quality metrics and raw grey matter fraction, we identified a relative reduction
149 of GABA+ levels in the older compared to the young, which was specific for both sensorimotor
150 voxels but not the occipital voxel.

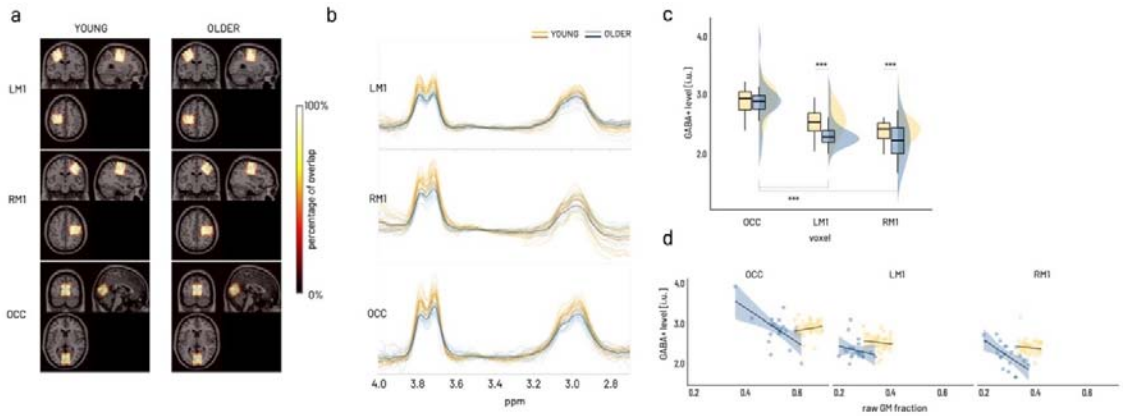

151
152 ***Figure 2 GABA MRS results.*** ***a)*** *Sum of individual GABA voxels projected into MNI space overlaid on standard brain*
153 *template. Color coding indicates overlay agreement in percentage of all available images within group. Neurological*
154 *display, i.e. coronal and axial view with left side on the left and right side on the right of image.* ***b)*** *Individual edited spectra*
155 *for LM1 (top), RM1 (middle), and OCC voxel (bottom) color coded for older (blue) and young (yellow) participants. Darker*
156 *lines present average spectra per group (orange – young, dark blue – older).* ***c)*** *Boxplots (see Material and Methods for*
157 *represented group statistics) and distributions shown for the interaction effect of group and voxel on GABA+, which is*
158 *driven by the differences between the occipital voxel and both sensorimotor voxels within the older in addition to the*
159 *between age group differences for both sensorimotor voxels. Asterisks indicate significant effects of model derived marginal*
160 *mean contrasts corrected for multiple comparisons at* ***p_{holm}*** *<.0001.* ***d)*** *Age-group specific effect of raw grey matter (GM)*
161 *fraction on GABA+ levels. Scatterplot (regression lines for subgroups with shading representing 95% CI) showing a relative*
162 *decrease in GABA+ levels with increasing raw GM fraction in the older across all voxels (p_{holm}<.0001). A high-resolution*
163 *version of this figure can be accessed under https://figshare.com/s/6ca09bf7c4185f3c3910*

164 ## Behavior

165 The control of transitions between motor-states was tested with a variation of an established paradigm
166 [18–21], in which the participants had to rhythmically tap in individually adjusted pace with the index and
167 middle fingers of both hands and to control transitions between two coordinative patterns of different
168 complexity (Figure 1a). The behavioral data collected during the performance of the behavioral
169 paradigm was analyzed in a time window of 2000ms following the 'switching' cue. The time window

of interest for these parameters was based on previous work [21] and pilot testing in older participants with the same task, which revealed that change in coordination mode is realized over an extended period. Furthermore, these previous results showed that a simple binarization of the precision (correct – wrong) does not reflect the ongoing adjustments made until the new coordination mode is mastered. Therefore, we aimed at quantifying performance with respect to (1) the precision (*error rate*) and (2) the speed (*transition latency*). Please see Methods for details about the behavioral paradigm and parametrization of outcome parameters. On average 119±20.5 trials of individual transitions per participant were subjected to the analysis including N= 21 young and N= 22 older participants (descriptive statistics given in Supplementary Table 5).

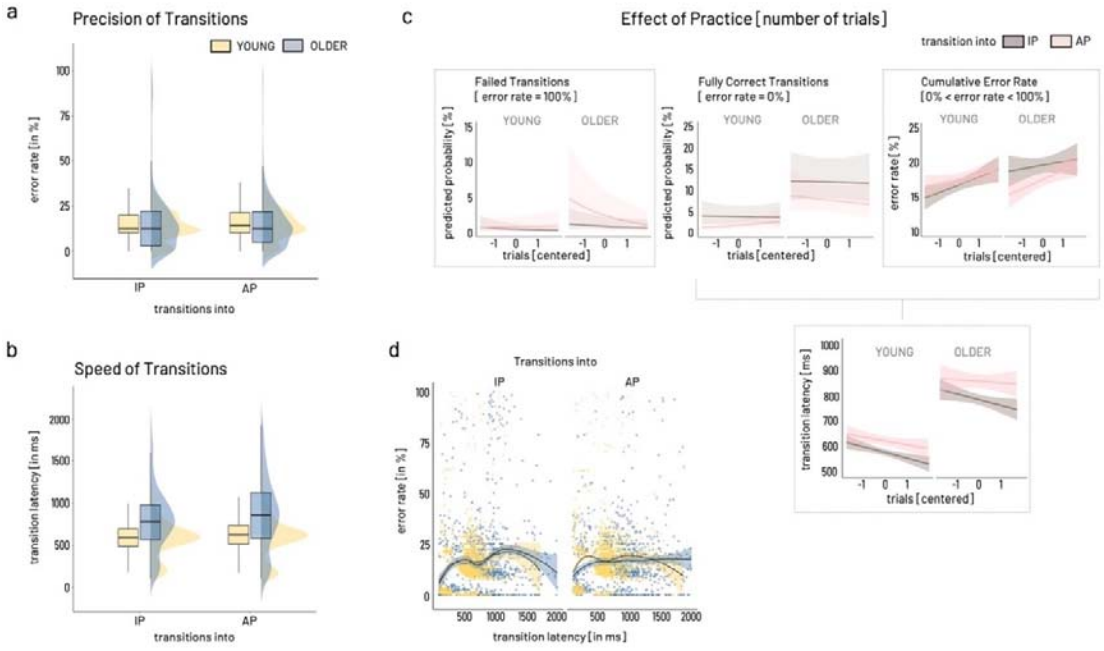

Figure 3 Predictors for behavioral outcome. a) *Error rate. Boxplots and distributions for overall error rate given separately for transition modes (IP: in-phase, AP: anti-phase) and age groups (blue: older, yellow: young).* ***b)*** *Transition Latency. Color coding as in a).* ***c)*** *Effect of practice, i.e. number of trials (depicted as centered variable), are given for Failed transitions (top left), Fully correct transitions (top middle), and Cumulative error rate (top right), and transition latency (bottom, failed transitions excluded). Brown indicates transitions into IP mode, light pink depicting transitions into AP. Frames around graphs indicate relevant modulation of the outcome over number of trials, i.e., for failed transitions, cumulative error rate, and transition latency. Only in the case of failed transitions, older showed a significantly different modulation over time for transitions into AP compared to the young with initially higher rate of trials with 100% error rate. Cumulative error rate showed a comparable increase across trials while transition latency decreased comparably in the two age groups and for both transition modes.* ***d)*** *For both groups and transitions modes (into IP, into AP), the relationship between speed and precision of transitions (excluding failed transitions) is non-linear as shown by locally weighted smoothing fitted over subgroups. A high-resolution version of this figure can be accessed under https://figshare.com/s/4620a8ad6c5dad113bd1*

Error rate

An overview of the distribution of error rate across age groups and transition modes is depicted in Figure 3a. To capture a comprehensive picture of performance during the transition phase, we chose to split the precision measure into three distinct levels, namely, *fully correct transitions* representing transitions showing 100% correct tapping, *failed transitions* reflecting transitions with 100% of erroneous tapping, and *cumulative error rate* consisting of all remaining transitions not considered fully correct or failed.

Failed transitions [trials with 100% error rate]. A logistic GLMM was used to predict failed transitions using group [OLDER, YOUNG], transition mode [IP, AP], and number of trials as independent variables (full results in Supplementary Table 6). With around 0.3%, the overall odds of completely failing a transition were low (intercept for group = young, nTRIALc = 0, transition mode = IP: $\beta = -5.66 \pm 0.60$ (odds ratio 0.003±0.002), 95% CI [-6.83, -4.49], $X^2 = -9.475$, $p < .0001$). Based on the Type II Wald statistics, trial number significantly modulated the occurrence of failed transitions in a transition mode specific way and distinct for both age groups (GROUP × TRANSITION MODE × nTRIALc, $X^2(1) = 4.4$, p=.04, Figure 3c left). Compared to the young, the older showed a higher number of failed trials early on and subsequently a steep decline of about 5% in likelihood of failed transitions from early to late trials for transitions into AP (odds ratio = -0.51±0.17, 95% CI [0.27, 0.96], $X^2 = -2.09$, $p<.05$). Independent of group, transitions into AP were twice as likely to fail than transitions into IP (odds ratio = 2.08±0.54, 95% CI [1.24, 3.46], $X^2 = 2.80$, $p<.01$, TRANSITION MODE Type II Wald $X^2(1) = 34.99$, $p<.0001$). Overall, with each additional trial, the odds of completely failing the transition tended to decline (odds ratio = 0.70±0.14, 95% CI [0.47, 1.04], $X^2 = -1.78$, p =.08, nTRIALc Type II Wald $X^2(1) = 9.86$, $p<.01$) irrespective of group or transition mode.

Fully correct transitions [trials with 0% error]. Similar to *failed transitions*, a logistic GLMM was fitted to predict fully correct transitions (full results in Supplementary Table 7). After removing failed transitions from the data, the overall odds for transitions to be fully correct were 4% (odds ratio = 0.038 for intercept: $\beta = -3.26 \pm 0.28$, 95% CI [-3.80, -2.72], $X^2 = -11.77$, $p < .0001$). Following the Type II Wald statistics, the two main explanatory parameters were GROUP ($X^2(1) = 15.43$, $p<.0001$) and TRANSITION MODE ($X^2(1) = 24.4$, $p<.0001$) and this was stable over number of trials. Remarkably, older participants were three times more likely to show completely correct trials (odds ratio = 3.52±1.25, 95%CI [1.76, 7.045], $X^2 = 3.6$, $p<.001$), irrespective of transition mode. Compared to transitions into IP, switching into AP was half as likely to result in fully correct transitions (odds ratio = 0.44±0.10, 95% CI [0.29, 0.69], $X^2 = -3.63$, $p < .001$) independent of group.

Cumulative error rate [0<error rate/100 <1]. A beta GLMM (logit link) was fitted to predict cumulative error rate including the same parameters as described above (full results in Supplementary Table 8). After excluding fully correct and fully erroneous transitions [0<error rate/100 <1], transitions between transition modes in either direction involved around 20% of erroneous tapping, i.e., cumulative error rate (intercept: $\beta = 0.21 \pm 0.04$, 95% CI [0.15 – 0.29], $X^2 = -9.07$, $p < .0001$). Based on the Type II Wald statistics, the two main parameters influencing cumulative error rate were number of trials (nTRIALc, $X^2(1) = 6.692$, $p<.01$) and TRANSITION MODE ($X^2(1) = 4.91$, $p<.05$). Investigating the parameter estimates revealed that cumulative error increased about 7% over the number of trials irrespective of group or transition mode ($\beta = 1.07 \pm 0.02$, 95%CI [1.02, 1.12], $X^2 = 2.87$, $p < .01$). In comparison to transitions into IP, switching into AP tended to yield around 6% higher cumulative error rate irrespective of group ($\beta = 1.06 \pm 0.03$, 95% CI [0.99 – 1.13], $X^2 = 1.78$, $p = .08$).

Transition Latency

The transition latency was defined as the time delay between cue onset and valid response, i.e. the first occurrence of the correct transition mode indicated by the cue. Accordingly, *failed transitions* were excluded from the trials for the calculation of the transition latency. An overview of the distribution of transition latency across age groups and transition modes is depicted in Figure 3b. A GLMM (Gamma family with a log link) was fitted to predict transition latency with the same independent variables described for error rate (full results in Supplementary Table 9). Given the model's reference categories, the average transition latency was estimated around 569 ms (intercept $\beta = 568.7 \pm 25.1$, 95% CI [521.68, 620.03], $X^2 = 143.98$, $p < .0001$). Based on the Type II Wald statistics, GROUP ($X^2(1) = 37.74$, $p<.0001$), TRANSITION MODE ($X^2(1) = 8.92$, $p<.01$), and number of trials (nTRIALc, $X^2(1) = 3.95$, $p<.05$) were the parameters explaining most of the transition latency's variance. The parameter estimates revealed, that older switched around 38% slower between transition modes compared to the young ($\beta = 1.38 \pm 0.08$, 95% CI [1.22, 1.55], $X^2 = 5.22$, $p < .0001$). Transitions into the AP pattern tended to be 7% slower than transitions into IP ($\beta = 1.07 \pm 0.04$, 95% CI [0.99, 1.17], $X^2 = 1.73$, $p = 0.08$). Independent of group or transition mode,

transitions tended to become around 4% faster over time (nTRIALc, β = 0.96±0.03, 95% CI [0.91, 1.02], X^2 = -1.37, p = .17).

In summary, the behavioral results for error rate and transition latency show an expected slowing of the older participants but both age groups showed a decrease in transition latency across the experiment. However, the results show no general age-group effect on the precision of transition performance. While older seemed to have a slightly higher rate of failing transitions into the more difficult AP mode early on, they showed an overall higher rate of completely correct transitions throughout the experiment compared to the young. The overall cumulative error rate, i.e. the percentage of erroneous taps in the course of a single transition, was comparable between the two age groups, showing an increase in errors as a function of practice (i.e., number of trials) and a trend of higher errors for transitions into the more challenging AP mode. Additional support for comparable transition performance in both age groups comes from the results of the thumb reaction task (methods and results in Supplementary Note 1, Supplementary Table 10), which neither show an effect of group nor interactions with transition mode or time across the experiment.

Finally, estimating the association between transition latency and error rate revealed a non-linear association of these two parameters for both age groups and transition modes (Figure 3d). For both groups and transition modes, the speed-precision association may roughly be approximated with an inverted-U shaped curve, potentially reflecting several underlying mechanisms beyond a linear speed-accuracy trade-off. Therefore, we argue that reducing the dimensionality of these two performance characteristics into one single measure appears not feasible. For subsequent analysis steps, trials of *fully correct transitions* and *cumulative error rate* were recombined into *error rate*, i.e. *failed transitions* were not considered for further analysis.

Task-related modulation of phase-based connectivity (ISPC)

Phase-related connectivity (inter-site phase clustering, ISPC) between motor-cortical source signals was analyzed in N=20 young and N=22 older participants (see Methods for details about participant inclusion).

Response-locked analysis of task and group related connectivity (ISPC) modulation.

No significant clusters were found for the interaction of group and transition mode. Subsequently, separate contrast analyses were performed to evaluate the effects of age group [YOUNG - OLDER] and transition mode [IP – AP].

Group Contrast [YOUNG – OLDER]

A cluster showing a significant relative decrease of connectivity between the homologue M1 sources was evident for the mu to high beta frequency ranges (12-38Hz) starting from -160ms and lasting until 220ms relative to the transition (Figure 4a). This effect was driven by a strong reduction in connectivity in the young while the older showed an increased connectivity overall but also when divided into separate time × frequency sub-clusters, reflecting pre-/post transition time zones and conventional frequency sub-bands. The sub-clusters spanned the ranges pre-transition high beta (-160 - 0ms, >25Hz), peri-transition low beta (-140 - 220ms,15-25Hz), and post transition mu frequency range (>120ms, 12-15Hz, Figure 4a, clusters A-C).

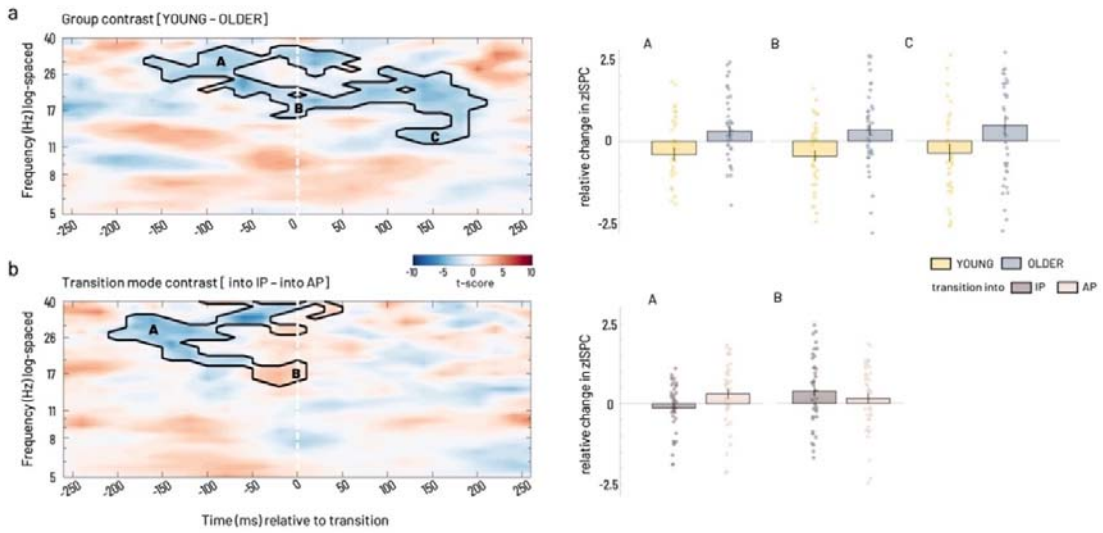

Figure 4 Statistical results of ISPC between left and right M1 source a) for group contrast time-locked to the individual mean transition time. *Cluster-corrected z maps for the test of GROUP contrast [YOUNG –OLDER, t-test against 0, p<.05 2-tailed]. Color coding in the time-frequency resolved zISPC plot indicates t-values. Dashed vertical lines at 0 ms on the time axis indicate the individual median latency, i.e. the time of transition. Bar plots present group averages of zISPC for respective cluster ranges, which were partly overlapping in time and frequency range for both, group and transition mode contrasts (black capital letters in the time-frequency plot correspond to black letters over bar plots), scatter plot depicts individual participants' data within group.* ***b) Statistical results for transition mode contrast time-locked to the individual mean transition time.*** *Cluster-corrected z maps for the test of TRANSITION MODE contrasts [into IP – into AP, t-test against 0, p<.05 2-tailed]. Bar plots show transition mode averages for respective cluster ranges. A high-resolution version of this figure can be accessed under https://figshare.com/s/11d01e6126cd7ba543de*

Transition mode Contrast [into IP – into AP]

For the cortico-cortical connection, a single cluster was visible, extending mostly in the pre-transition time window in the mu to high beta range (Figure 4b). Between -200 and 0ms, a relative decrease in the full beta range (20-35 Hz) was evident (cluster A). This effect was driven by a decoupling before transitions into IP, while transitions into AP were rather associated with an increase in M1-M1 connectivity before the actual transition was accomplished. Around the time of the transition, -50 – 60ms, a relative increase in connectivity expanded over mu to beta range (cluster B), which was caused by an increased coupling for transitions into IP compared to transitions into AP.

Taken the results of both contrasts together, interhemispheric motor-cortical connectivity showed clear age group differences in its spectral features during transitions. Furthermore, a modulation by transition mode (into IP versus into AP) was also visible but we did not find evidence for altered connectivity in the older participants that was specific for transitions into one of the two transition modes but rather a general change in connectivity pattern in the older adults.

Single-trial phase angle difference – behavior association

Our next interest was to further investigate the association between interhemispheric interactions and behavior. Because inter-site phase clustering (ISPC) is calculated over trials, no inference can be made about the intra-individual variations of the inter-site phase relationship and its association with variations in behavior. Linking inter-site interactions and behavior on a trial-by-trial basis allows to interpret the signature of this association and draw conclusions about the behavioral relevance of the neural mechanisms. Therefore, frequency-specific phase angle differences between left and right M1 were extracted for each trial at the respective trial-based time of transition for the low (15-22Hz) and high beta (25-30Hz) frequency ranges identified in the respective time × frequency clusters during the previous analysis step (Figure 4).

In order to explore the role of the endogenous GABA+ concentration on this relationship, we dichotomized GABA+ concentration into below and above within group median concentration. Two-way ANOVA results showed that the factor group was a major source of variance for the average

329 angle and that this was modulated by GABA+ level for both frequency ranges (***15-22Hz***: GROUP
330 $X^2(2) = 99.22$, p<.0001, GABA+ $X^2(2) = 4.14$, p = .13, GROUP × GABA+ $X^2(1) = 4.10$, p=.04; ***25-***
331 ***30Hz***: GROUP $X^2(2) = 19.86$, p = 4.9e-05, GABA+ $X^2(2) = 8.75$, p=.013, GROUP × GABA+ $X^2(1)$
332 = 9.99, p = .0016 (see Figure 5, additional results are given in Supplementary Note 3, Supplementary
333 Table 11). Whereas, transition mode alone did not account for the variance in the data (***15-22Hz***:
334 TRANSITION MODE $X^2(2) = 0.57$, p = .8, GABA+ $X^2(2) = 4.14$, p = .13, TRANSITION MODE ×
335 GABA+ $X^2(1)= 5.38$, p = .02; ***25-30Hz***: TRANSITION MODE $X^2(2) = 4.16$, p = .13, GABA+ $X^2(2)$
336 = 8.75, p = .013, TRANSITION MODE × GABA+ $X^2(1) = 2.85$, p = .09). For both frequency ranges,
337 circular-linear correlation revealed a significant association between phase-angle differences and
338 quality of performance (i.e. error rate) following the transition. This association pattern was distinct
339 for the two age groups in dependence of the relative (lower versus higher) GABA+ concentration.
340 Specifically, when pooled over transition modes, phase angle differences were significantly associated
341 with subsequent performance in the older adults in the low GABA+ subgroup. In the young, in
342 contrast, a significant association was found for the high GABA+ subgroup (15-22Hz: $OLDER_{high\ GABA+}$ rho = 0.03, p_{FDR}= .5, $YOUNG_{high\ GABA+}$ rho = 0.08, p_{FDR}= 5.45e-10; $OLDER_{low\ GABA+}$ rho = 0.07,
344 p_{FDR}= 5.45e-10, $YOUNG_{low\ GABA+}$ rho = 0.02, p_{FDR} = .7; 25-30Hz: $OLDER_{high\ GABA+}$ rho = 0.03, p_{FDR}=
345 .9, $YOUNG_{high\ GABA+}$ rho = 0.07, p_{FDR}= .0005; $OLDER_{low\ GABA+}$ rho = 0.06, p_{FDR}= .007, $YOUNG_{low\ GABA+}$ rho = 0.04, p_{FDR}= .2). Plotting error rate as a function of phase angle differences shows a
347 variation in the trend of this association along the range from -360˚ to +360˚ phase lag, i.e. explaining
348 the overall small correlation coefficient (Figure 5c, d). Specifically, for both subgroups (older with
349 lower GABA+, young with higher GABA+), a behavioral advantage for phase angle differences
350 around 0˚ and higher subsequent error rate with phase angle differences of -180˚ and 180˚ were found.

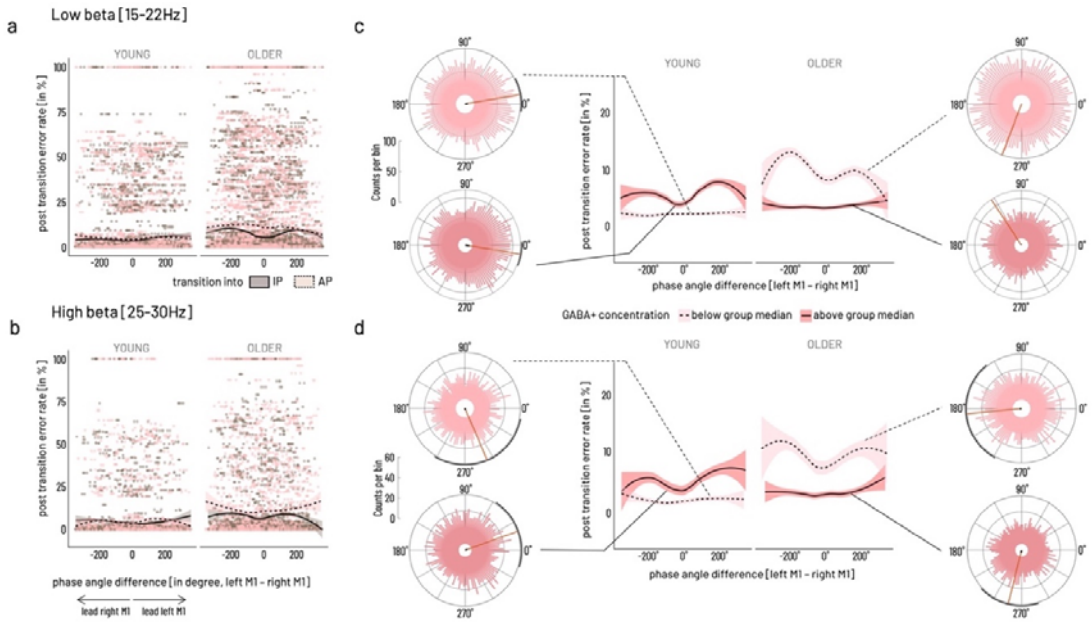

Figure 5 Association between cortico-cortical phase angle differences at the time of transition and subsequent performance error a) *in the low beta [15-22Hz] range* ***b)*** *in the high beta range [25-30Hz]. Data points represent single trial data for transitions into IP (brown) and into AP (light pink) mode, solid line indicates average phase angle difference – behavior association during transitions into IP mode, dashed line indicates average phase angle difference – behavior association for transitions into AP mode.* ***c)*** *Mean phase angle differences were significantly modulated by factors age group and relatively higher versus lower GABA+ concentration when binarized into above (dark red shading, solid lines for subsample mean) versus below group median (light pink shading, dashed lines for subsample mean) in the low and* ***d)*** *in the high beta frequency band. Rose plots show histogram of binned phase angle differences with mean direction (red line) and 95% CI (black circumference) for significant non-uniformity of distribution. Phase angle differences for the low and high beta band were significantly associated with subsequent performance error in the young with relatively higher and in the older with relatively lower motor-cortical GABA+ concentration. In these subgroups, close to 0˚ phase lag was behaviorally beneficial (lower errors), while close to 180˚ phase lag was associated with higher performance errors. A high-resolution version of this figure can be accessed under https://figshare.com/s/7b43133df22f84496168*

To validate the specificity of the effects in terms of task-context and topography, the same analysis steps were run for two control conditions, namely the LM1-RM1 phase lag at a random time point during baseline [start cue – 300ms], i.e. during between-trial pauses (Figure 1b), and for phase angle differences for the OCC-L/RM1 connectivity at the time of transition. The analyses of the two control conditions revealed a significant GROUP x GABA+ modulation of the mean direction of phase angle differences between left and right motor cortical sources during the within-trial baseline [start cue -300ms]. Furthermore, it showed a significant association between baseline phase lag and performance in the subsequent trial. While this association broadly resembled the pattern during transition described above, it was less specific for the within-age group GABA level in the low beta range (descriptive and inferential statistics in Supplementary Tables 12-14, Supplementary Figure 3).

While we also found a significant GROUP x GABA+ modulation of the mean direction of the phase angle differences between the occipital source and both motor cortical sources at the time of transition for both frequency ranges, the pattern of the mean direction clustering was clearly different from that of the interhemispheric motor-cortical interaction in that it was not involving the clustering around 0˚ and 180˚. Finally, no association between occipital – primary motor phase lag and behavioral performance was found (OCC-LM1 and OCC-RM1 all p_{FDR}>.1, descriptive and inferential statistics in Supplementary Tables 15-18, Supplementary Figure 4).

In summary, single trial phase angle differences at the time of transition showed to be different between the age groups and this effect was influenced by level of motor-cortical GABA+ concentration. While in the young, the association between phase angle difference at time of transition and subsequent performance error was stronger under the relatively higher GABA+ concentration subgroup, the older showed a stronger association in the relatively lower GABA+ concentration subgroup. In both cases, 0˚ phase lag represented a behaviorally more advantageous state whereas a 180˚ phase lag was associated with more subsequent errors. This association was specific for the interaction between left and right primary motor sources and for the time of transition.

Association between behavior and connectivity through GABA+

In order to test the impact of baseline GABA+ levels on the relationship between interhemispheric motor-cortical connectivity and behavior in addition to the effect of age on the associations among all three variables (see Methods for details, schematic model structure given in Figure 1a on the right), we employed a Bayesian moderated mediation analysis. For this purpose, we modelled the ISPC values extracted from the significant time × frequency sub-clusters of the response-locked analysis (independent variable), the median transition latency or error rate (dependent variable), the respective GABA+ (mediator), and age (moderator) and estimated their associations in separate models for each of the individual connectivity pairs. Because all input variables were centered prior to modelling, it is necessary to keep in mind that conditional effects consequently need to be interpreted relative to the respective age group mean. As shown in the results below, for all significant models (see Figure 6a

for an overview), age was a relevant effect moderator of all model paths in the case of error rate and transition latency (Figure 6b, c). Hence in the subsequent step, mediation results are shown conditional on the moderator age, highlighting predominantly opposing trends in the two age groups (regression coefficients for separate model paths given for all Bayesian moderated mediation models in Supplementary Table 19).

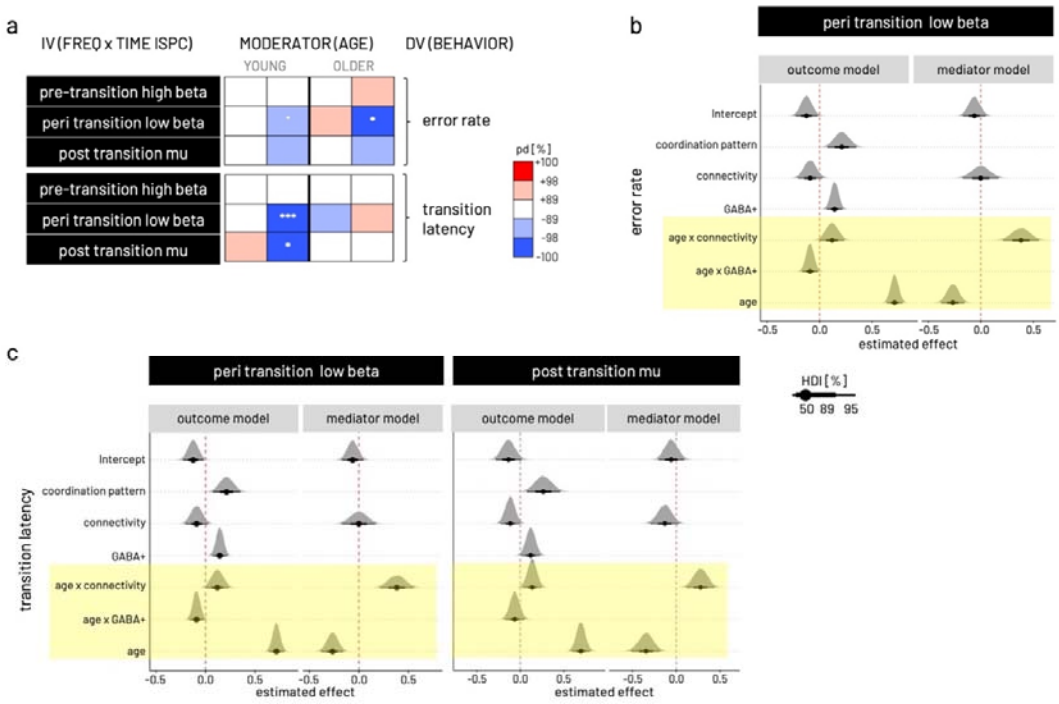

Figure 6 Results of Bayesian moderated mediation models. a) *Overview over posterior directions (pd) for indirect (mediation) effects on error rate (upper matrix) and transition latency (lower matrix) conditional on upper/lower quintiles of moderator age (depicted as YOUNG and OLDER) for the models estimated with the independent variable (IV) based on the three time × frequency clusters derived in the response-locked ISPC analysis. Color coding of pd represents likelihood (in %) and direction of effect, i.e. red shading for positive effects and blue shading for negative effects. A pd of 95, 97.5, 99.5, and 99.95% corresponds to the frequentist 2-sided p-value at the thresholds 0.1˚, 0.05*, 0.01**, 0.001*** respectively.* ***b)*** *Probability density plots for effects of parameters in the outcome and the mediator models input to the mediation analysis. Depicted are the three models with significant mediation shown in a). Outcome model shown for error rate and peri transition low beta ISPC.* ***c)*** *Outcome models shown for dependent variable transition latency and peri-transition low beta ISPC (left) as well as post transition mu ISPC (right). For all three models shown in b) and c), the mediator model is related to right M1 GABA+. Highlighted in yellow are the significant effects of moderator age in all three models indicated by the posterior distributions of respective parameters falling with >99.5% on one side of the red dashed vertical line. Linewidth of black horizontal bars indicate 50, 89, and 95% highest density interval [HDI] of the parameters' effect. A high-resolution version of this figure can be accessed under https://figshare.com/s/d6c5c42fa8395c4a779b*

421 ***Connectivity significantly predicts behavior in a time and frequency specific manner and this***
422 ***relationship is moderated by age.*** The main results for the models estimating the association between
423 connectivity and behavior are graphically summarized in Figure 6a for cumulative error rate and
424 transition latency. Generally, models including right hemispheric GABA+ levels yielded stronger
425 evidence for mediation effects than those including left hemispheric GABA+ for both age groups.
426 Overall, the young group showed stronger evidence for mediation effects than the older.

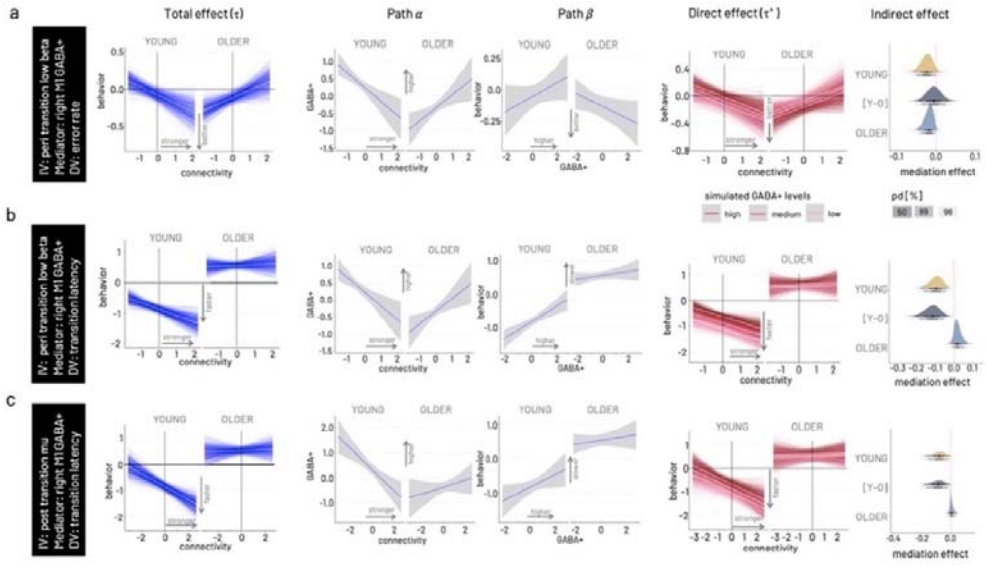

427

428 ***Figure 7 Results of Bayesian moderated mediation models.*** *From left to right, total effect (path τ) conditional on moderator*
429 *age, association between connectivity and GABA+ (path α), association between GABA+ and transition latency (path β),*
430 *simulation of the mediation effect on the connectivity – behavior association (direct effect, path τ') for varying levels of*
431 *GABA+ (low – light pink, medium – red, high – dark red), and probability density ploy for the mediation effect conditional*
432 *on age including the difference of young versus older [Y-O] mediation effects. In all three models, right hemispheric GABA+*
433 *concentration is modelled as mediator.* ***a) Model for peri-transition low beta connectivity – error rate association****. As*
434 *visible in the total effect, the young behaviorally benefit from stronger M1-M1 connectivity in the low beta range, while the*
435 *older show higher errors with stronger connectivity. The association between connectivity and GABA+ (path α) shows*
436 *opposing trends in the two age groups, a negative association in the young and a positive association in the older. The*
437 *association between GABA+ and transition latency (path β) is positive in the young and negative in the older. Simulations*
438 *for the full moderated mediation model show that for the young the positive behavioral effect of stronger connectivity is*
439 *more pronounced in the presence of relatively lower GABA+, while for the older the negative effect of increased connectivity*
440 *is ameliorated in the presence of higher GABA+. Probability density plots of the mediation effect conditional on age for this*
441 *model show a negative indirect effect for both age groups, and no difference between the age groups. Grey shading of*
442 *probability of direction (pd) indicates limits of 50, 89, and 98% CI.* ***b) Model for peri-transition low beta connectivity –***
443 ***transition latency association. c) Model for post-transition high mu connectivity – transition latency association****. A high-*
444 *resolution version of this figure can be accessed under https://figshare.com/s/e7c918da53dbc9d5ea3f*

Stronger connectivity makes the young – but not the older – adults perform better. Simulating the total effect, i.e. the association between connectivity and behavior, conditional on moderator age reveals the opposing effects within the two groups (age group comparison depicted for one example model in Figure 7a). For all three time by frequency clusters, the young participants show strong evidence that relatively stronger connectivity is associated with better performance, i.e. lower (i.e. relatively faster) transition time (pd = 100%) and lower error rate (pd = 100%, except pre-transition beta). In contrast, within the older adults, relatively stronger connectivity is associated with a relative slowing in transition latency (pd 100%) but also with a trend for lower error rate (pd >89%, except post-transition mu).

Older adults benefit in precision from higher non-dominant GABA+ levels. For the association between connectivity in the peri-transition low beta band and error rate, both young (pd >95%) and older (pd >98%) show a negative indirect effect of right M1 GABA+ levels. This negative mediating effect has diverging consequences on behavior for the two age groups (Figure 7a). In the young, the association between relatively stronger coupling and better performance, i.e. lower error rate, was more pronounced in the presence of lower non-dominant GABA+ concentration. In the older, on the other hand, connectivity variations had a stronger impact on behavior, i.e. stronger coupling led to relatively higher error rates, in the presence of lower GABA+ concentration. In contrast, the association between stronger coupling and worse performance, i.e. higher error rate, was ameliorated in the presence of higher right M1 GABA+ concentration in the older.

Young adults are faster with higher connectivity in the presence of lower non-dominant GABA+. Simulating the mediation effect conditional on the moderator age, revealed a negative indirect effect of right hemispheric GABA+ (pd >98-100%) on the association between connectivity on both behavioral outcomes, transition latency and, to a weaker extent (pd >89-95%), on error rate in the young. Specifically, in the presence of lower right M1 GABA+ levels, the negative association between peri-transition low beta and transition latency was steeper in the young, i.e. in the presence of low GABA+ levels, stronger connectivity was associated with generally faster transitions while this effect was less pronounced in the presence of high GABA+ levels (Figure 7b). This effect was comparable for connectivity in the high post-transition mu range and transition latency (Figure 7c). The mediation effect between connectivity and transition latency was absent in the older for all time by frequency clusters (Figure 7b, c). This absence of an indirect effect in the older can be explained by a weak association between the post-transition mu connectivity and GABA+ (path α) and in particular the absence of an association between right-hemispheric GABA+ and transition latency (path β) in both models.

In summary, the multimodal data fusion analysis revealed four main findings with respect to the potential mediating role of baseline GABA+ on the association between connectivity and behavior. First, baseline GABA+ levels exert an indirect effect on the link between interhemispheric motor-cortical connectivity in the low beta and high mu frequency band, time-locked to the behavioral event, and behavior. Second, variations in non-dominant hemispheric (right M1) GABA+ concentration was more likely to exert an indirect effect as compared to dominant hemispheric sensorimotor GABA+ concentration. Third, individual variations in baseline GABA+ were found to exert an indirect effect in the young for models with speed and error rate, whereas an indirect effect for the older was only found in the model with error rate. Fourth, although the mediating effect of individual variations in baseline GABA+ is of the same direction in both age groups, it has diverging implications for the connectivity – behavior association in young and older adults. Importantly, the latter two points underline the overall expected finding of age being a strong effect moderator for mostly all bimodal relationships investigated here.

Discussion

To flexibly adjust ongoing behavior and switch between different modes of action is an essential ability in the human behavioral repertoire. Unfortunately, this flexibility declines across cognitive domains with increasing age [1]. Using a multimodal approach to investigate the interplay between endogenous GABA and the brain's responsiveness during dynamic motor state transitions, a prototype of flexible behavior, we provide converging evidence to suggest age-related differences in the preferred state of endogenous GABA+ concentration to allow for interregional neural communication and benefit behavior. We are able to draw conclusions about the character of the neural and neurochemical findings with regard to age-related compensatory mechanisms versus deterioration.

Interhemispheric interactions at time of transition predict subsequent performance precision

While the unimodal results highlighted the specific sensitivity of GABA+ concentration and phase-based interhemispheric motor-cortical connectivity to aging-related alterations, even in the absence of fundamental performance differences between the age groups, the evolving question became how the age-related changes may be expressed and reflect the underlying mechanisms of behavior. Consequently, we linked inter-site interactions in the beta frequency range, detected in the unimodal analysis of connectivity at the time of transition, and behavior on a trial-by-trial basis. This analysis revealed an age-group-specific modulation of the interhemispheric phase lag between primary motor sources at the time of transition in addition to its association with the subsequent performance error. In an exploratory analysis, we found a first indication that phase lag at the time of transition and its association with subsequent behavior varied in dependence on the GABAergic state. Specifically, while in the young adults, relatively lower (than median GABA in the young) motor-cortical GABA+ concentration generally co-occurred with better performance irrespective of phase lag, relatively higher (than median GABA in the older) motor-cortical GABA+ concentration co-occurred with overall better performance in the older. In the respective less advantageous GABAergic state (i.e.,

516 relatively higher GABA+ in the young and relatively lower GABA+ in the older), 0˚ phase lag at the
517 time of transition was followed by better performance, whereas a 180˚ phase lag was associated with
518 more subsequent errors. These findings suggest a behavioral advantage through synchronization of
519 interhemispheric primary motor sources with a phase lag of around 0˚. Even though we may not rule
520 out effects of volume conduction and source leakage on the inter-site phase relationship [22], we were
521 able to confirm our results' temporal and regional specificity by comparing the interhemispheric
522 motor-cortical phase lag during the transition with that at baseline and with the occipital-motor
523 interaction. Previous work has suggested zero-phase lag for long-distance connectivity in the beta
524 frequency range between sensors covering left and right motor cortices during resting-state, as studied
525 with magnetoencephalography [23]. Additional support for our findings' cogency comes from recent
526 work that has proven the omnipresence of broadband zero-lag (i.e., 0˚ and 180˚ phase difference)
527 functional connectivity, specifically for the homotopic brain regions based on intracranial recordings
528 during varying vigilance levels in humans [24]. Although both studies have investigated spontaneous
529 oscillations during resting-state, the authors speculated that functional connectivity around 0˚ phase
530 lag might serve as a fundamental mechanism for the instantaneous integration of information from
531 across brain regions allowing for predictive coding of expected events. Precisely, through long-
532 distance synchronized oscillatory activity, the motor system might facilitate the anticipation of
533 intrinsic or extrinsic cues allowing it to act with higher temporal precision. While our data support this
534 hypothesis by showing a behavioral advantage of 0˚ phase lag at the time of transition, we also found
535 an association between 0˚ phase lag during the within-trial baseline with performance of the
536 subsequent trial, though less frequency-specific. During the within-trial baseline, the participants were
537 required to remain attentive to the fixation cross and await the 'start cue'. Therefore, this observation
538 suggests that the interhemispheric zero-lag synchronization might represent a more global state to
539 potentially support the preparedness of the motor system. A mechanism to better anticipate the
540 required behavioral action may have been specifically relevant in a less-well tuned system, i.e., less
541 beneficial GABAergic state, and may represent a compensatory mechanism to uphold behavior.

General age-gradient and hemispheric asymmetry of GABA+ concentration

To further investigate the indirect effect of GABA+ concentration on the relationship between phase-based connectivity and behavior, we used a Bayesian moderated mediation analysis integrating all three modalities. This analysis step confirmed on the one hand a steep age gradient for all bimodal interactions, i.e., all paths within the model, rendering the mediation analysis conditional on the moderator age highly meaningful. On the other hand, it revealed a hemispheric asymmetry of the mediator GABA+. Specifically, modelling the right hemispheric GABA+ concentration yielded higher evidence for an indirect effect on the connectivity-behavior relationship as compared to the GABA+ concentration of the left hemisphere. Given the non-directedness of the connectivity measure and the bimanual nature of the behavioral outcomes used here, the only variable differentiating hemispheric laterality is the mediator. While we did not find a hemispheric difference in sensorimotor GABA+ concentration in either group in the unimodal analysis, the Bayesian model was sensitive to the actual variance. Previous MRS data from our own group support a hemispheric asymmetry in sensorimotor GABA+ concentration with lower concentration in the non-dominant hemisphere [25,26]. Electrophysiological data evidences an imbalance of phasic and tonic GABAergic inhibitory mechanisms within the motor system, also reflecting reduced fine-tuning of the non-dominant hemisphere across various age groups (e.g. [27–29]). Therefore, it is conceivable that the less well-tuned non-dominant hemisphere is more susceptible to excitation-inhibition variations and hence has a more pronounced effect on time-sensitive neural communication relevant for behavior, as suggested by our mediation results, irrespective of age. In addition to these two general findings, the mediation analysis delivered converging evidence for the two diverging states of beneficial GABA concentration in the two age groups as already suggested by the single-trial analysis of the phase angle differences.

Relatively lower endogenous GABA+ reflects the optimally tuned young neural system.

We found an indirect effect of non-dominant GABA+ concentration on the connectivity – behavior association for both speed and precision in the young subgroup. In the presence of lower

GABA+ levels, relatively stronger peri-transition beta band and post-transition mu band coupling (i.e., less decoupling) was associated with better performance. This association weakened in the presence of higher GABA+ concentration in the young. Notably, the young showed overall higher GABA+ levels than the older for both motor cortex voxels. Hence, when interpreting the relative GABA+ concentration in the young, even lower levels are still comparably higher than the average seen in the older.

Computational modeling supports that extra-cellular GABA levels, most likely primarily detected with MRS [30,31], are critically influencing the variability in cortical neural activity and thereby define adequate information processing and integration [32]. Previous in vitro and in vivo work from animal models suggests that low extracellular GABA+ concentration represents the fine-tuned physiological environment with the optimal inhibitory tone for efficient and timely precise up- and down-regulation of phasic synaptic inhibition (reviewed in [33]). In support of these findings, experimental elevation of GABA+ concentration has shown to cause disturbances of neural processing, perception, and behavior in young healthy volunteers. Hereof, pharmacologically increasing endogenous GABA beyond physiological levels has shown to lead to exaggerated amplitudes of early evoked responses in somatosensory cortical areas [34] and decreased amplitudes of medium-latency evoked responses in the visual cortex [35]. Previous findings of elevated GABA concentration affecting both phasic and tonic inhibitory signaling of pyramidal and inter-neuronal cell populations in superficial and deep cortical layers may serve as a potential explanation [36–38]. While it is worth noting that lowering GABAergic concentration below physiological levels also has shown to cause acute disturbance of spontaneous neural activity and perceptual processing in the primary visual cortex in young macaque monkeys [39,40], additional evidence for the detrimental functional effects of elevated GABA levels is available for sensorimotor processing. Strengthened movement-related desynchronization in the beta-frequency range detected over the primary motor cortex has been specifically linked to pharmacologically increased GABAergic drive [41]. In this former work, local desynchronization in sensorimotor beta-band oscillations, instead of peri-movement gamma-band or post-movement beta-band synchronization, was critically susceptible to pharmacological

595 manipulation with benzodiazepines. In the present work, we found the indirect effect of GABA to be
596 frequency-specific for response-locked modulation of long-distance synchronization in the mu and
597 beta frequency range and its association with performance.

598 We therefore argue that the relatively lower endogenous GABA levels in the young reflects
599 their neural system's preferred inhibitory state for effective neural communication, which assures the
600 required responsiveness to modulate inhibition in the presence of dynamic task requirements.

601 **Higher GABA+ indicates neural system integrity and better functioning in the**
602 **older adults.**

603 In older adults, evidence for an indirect effect of GABA+ was restricted to the association between
604 peri-transition beta-band connectivity and error rate. While the indirect effect of baseline GABA+ was
605 negative as in the young, the implications for the connectivity – behavior association were the
606 opposite as compared to the young. The detrimental effect of higher beta band connectivity on
607 performance error in the older was ameliorated in the presence of higher GABA+ levels. In contrast to
608 the young, relatively higher endogenous GABA appeared to represent the behaviorally more
609 beneficial state in the older adults. This finding is, at first sight, intriguing, and the question is why the
610 older do not benefit from the relatively lower GABA+ levels in the same way the younger adults do?
611 However, retaining relatively higher GABA+ levels, i.e. closer to the concentration found in the
612 young, probably reflects less age-related decline and subsequently lower impact on time-sensitive
613 modulation of neural communication. Along these lines, higher GABA+ concentration has been
614 suggested to promote lower errors through optimal tuning of neural activity (reduced variability),
615 promoting a better signal-to-noise ratio in the older. One effect of higher signal-to-noise is a more
616 efficient perceptual filtering function from lower to higher level processing stages. A growing body of
617 results from animal models (e.g. [39,40]), computational modeling [32,42], as well as results from aging
618 human volunteers (e.g. [43]) supports this hypothesis. From this perspective, the mediating effect of
619 GABA levels on the association between peri-transition beta-band connectivity and performance
620 precision but not performance speed in older adults, as seen here, appears conceivable.

The interhemispheric connectivity in the present study was modulated on a level of overall increased coupling in the older, whereas in the young a relative decoupling was observed throughout the motor-state transitions, which can be interpreted within the hypothesis of age-related dedifferentiation (e.g. [44,45]). Previous work has shown reduced endogenous GABA+ levels to be linked to decreased resting-state network segregation, i.e., increased connectivity, and lower sensorimotor performance in older adults [12]. Although controversial findings exist, an increased interregional coupling has frequently been observed across imaging methods in older populations during task-free [46,47] and task-related conditions [48,49].

The question as to whether alterations in GABAergic transmission reflect the cause or the 'cure' (i.e., compensation) for age-related neuronal functional decline reflected in behavioral performance deficits remains yet to be fully answered. In view of the limitations of the present work, it is necessary to point out that strictly speaking, a mediation implies the assumption of direct causality, which was not upheld in the present cross-sectional study. Considering the collision or confound of many other factors modifying age-related changes of the brain-behavior interaction neglected here, our findings highlight the importance to investigate the nature of the interactions as a function of age. Finally, our Bayesian moderated mediation analysis, though hypothesis-driven, followed an exploratory approach and we acknowledge the lack of a cross-validation. Nonetheless, based on the converging evidence from our multimodal analyses, we conclude by proposing the increased interhemispheric connectivity to represent a compensatory mechanism, which is brought about by rhythmic entrainment of neural populations in homotopic motor cortices. Through this increased (potentially zero-lag) synchronization, the motor system is in a better state to anticipate and dynamically control motor action. This mechanism appears to be readily available in the young and healthy brain but seems to be most relevant in the presence of a less optimal tuning of the inhibitory tone to uphold the required dynamics of behavioral action as seen here in the older.

Materials and Methods

Ethics Statement

The protocol and all procedures of this study complied with the ethical requirements in accordance with the Declaration of Helsinki in its revised version from 2008, as approved by the medical ethical committee of the KU Leuven (local protocol number S-58811, Belgian registration number B322201628182). All participants gave written informed consent to all of the study's experimental procedures and were reimbursed with 15 € per hour.

Participants

44 volunteers (older group N = 22, age range 62-82 years of age; young group N = 22, age range 21 – 27 years of age) were recruited through local advertisements and were screened for in- and exclusion criteria. No statistical method was performed for an a priori sample size calculation; rather, we based reasoning for the selected sample size on numbers chosen in previous multimodal work (eg. [12]). One young participant dropped out after the MRI data acquisition for personal reasons unrelated to the study. MRI, EEG, and behavioral data were thus collected in 21 young (10 women) and 22 older (11 women) participants. Due to technical problems, the EEG of one young participant had to be excluded, yielding different numbers of data sets included into the analysis for GABA, behavioral, and EEG analysis. All participants were right-handed, as evaluated with Edinburgh Handedness Inventory [50] (laterality quotient: older 92.50±0.20, young 85.00±0.15, median±95% CI). All participants were free from neurological impairments and musculoskeletal diseases affecting the unconstrained movement of the fingers, did not take neuroactive drugs, and had normal or corrected-to-normal vision as evaluated with an in-house standardized questionnaire.

Magnetic Resonance Imaging (MRI) and Magnetic Resonance Spectroscopy (MRS) acquisition

MRS data acquisition and reporting was done following the Magnetic Resonance Spectroscopy quality assessment tool (MRS-Q) [51]. A 3D high-resolution T1-weighted structural image (repetition time = 9.5 ms; echo time = 4.6 ms; voxel size = 0.98 x 0.98 x 1.2 mm^3; field of view = 250 x 250 x 222 mm^3; 185 coronal slices) was acquired for each participant using a Philips Achieva 3.0T MRI system and a 32-channel head coil. The 30x30x30mm^3 MRS voxels were positioned based on the T1-weighted image. For the left and right sensorimotor voxels, this was centered above the hand knob area [52] and rotated in the coronal and sagittal planes to align with the cortical surface of the brain. The occipital voxel was medially centered over the interhemispheric fissure, with the inferior boundary of the voxel aligned in parallel to the Tentorium cerebelli to cover left and right occipital lobes symmetrically [53].

Data were acquired using the Mescher–Garwood point resolved spectroscopy (MEGA-PRESS) sequence [54], with parameters resembling those of previous work [15–17]; 14ms sinc-Gaussian editing pulses applied at an offset of 1.9 ppm in the ON experiment and 7.46 ppm in the OFF experiment, TR = 2000ms, TE = 68ms, 2000 Hz spectral bandwidth, MOIST water suppression, 320 averages, scan duration of 11 minutes, 12 seconds]. Sixteen water-unsuppressed averages were acquired from the same voxel. These scan parameters were identical for all three voxels.

MRS data were analyzed with the Gannet software 3.0 toolkit [55]. Individual frequency domain spectra were frequency- and phase-corrected using spectral registration [56] and filtered with a 3Hz exponential line broadening. Individual ON and OFF spectra were averaged and subtracted, yielding an edited difference spectrum, which was modelled at 3ppm with a single Gaussian peak and a 5-parameter Gaussian model. The unsuppressed water signal serving as the reference compound [57], was fit with a Gaussian-Lorentzian model. The integrals of the modelled data were then used to quantify the uncorrected GABA levels. As discussed extensively, this method edits GABA as well as macromolecules at 3 ppm [58,59], therefore GABA levels reported are referred to as GABA+ (i.e., GABA+ macromolecules). To adjust GABA+ levels for heterogeneity in voxel tissue composition,

MRS voxels co-registered to the high-resolution anatomical image were segmented into three different tissue classes, namely gray matter (GM), white matter (WM), and cerebrospinal fluid (CSF), with SPM 12 (http://www.fil.ion.ucl.ac.uk/spm/software/spm12/). The resulting voxel compositions were used to extract tissue-corrected GABA+ following the assumptions that GABA+ levels are negligible in CSF and twice as high in GM relative to WM [60], accounting for tissue-specific relaxation and water visibility values [60]. GABA+ levels were normalized to the average voxel composition within each age group after outlier removal [60]. Quality of the MRS data was assessed using the quantitative metrics GABA and the N-acetylaspartate signal-to-noise ratio (GABA SNR, NAA SNR), fit error of the GABA peak (GABA Fit Error), the drift (Drift) and the standard deviation of the water frequency offset (Frequency Offset), as well as linewidth, quantified as the full-width half-maximum of the modelled and N-acetylaspartate (NAA FWHM) signal.

Behavioral Paradigm

The behavioral task involved two transition modes representing the two motor states, i.e. a mirror-symmetric synchronous tapping of homologue fingers (in-phase, IP, the more stable motor state) and a synchronous tapping of the index and middle finger of opposite hands (anti-phase, AP, the less stable motor state). Since the AP transition mode has been shown to represent the coordinatively more challenging pattern [13,18,61], tapping frequency was individually adjusted to 80% of the frequency with which the AP pattern was comfortably performed without involuntary spontaneous transitions into the IP transition mode. This individual tapping frequency was auditory paced throughout the complete experiment. During the EEG session, the auditory pacing stimulus was provided through insert etymotic earphones with flat frequency response (Cortech Solutions, Wilmington, NC, USA). Tapping was performed on a custom-made keyboard with six input keys (1000Hz sampling rate). Visual target cues were presented on a standard 19” computer screen (refresh rate 60Hz) and indicated which movement pattern to perform. Visual and auditory stimuli of the behavioral paradigm were programmed in LabVIEW 2016 (National Instruments, Austin/TX, USA). One complete trial consisted of a start cue subsequently followed by a cue to either continue with the same transition

719 mode ('continuation') or transition into the respective other pattern ('switching' from IP to AP, or
720 vice versa, Figure 1a). In this study, we focused on the switching transitions and thus the ratio of
721 occurrence of continuation versus switching transitions was set to approximately 1:5 to yield enough
722 trials for further analysis and keep participants from automatically switching. Trials were interleaved
723 with pauses ('pause'), which were always of the same length (3000ms); the other events had a jittered
724 inter-stimulus interval (5000-8000ms). In order to preserve attention at a high level throughout the
725 experiment, an additional thumb reaction time task (tRT) was included, which could occur instead of
726 any other event type with a chance of 5%. The instruction was to respond as fast as possible upon cue
727 occurrence (a magenta circle on left or right side of fixation cross) indicating either the left or right
728 thumb to press the respective key. The tRT task was always followed by a pause with a latency of
729 1000ms to avoid interference with transition performance. In order to minimize eye movements,
730 participants were instructed to fixate a small cross in the center of the screen, which was visible at all
731 times, during and in-between all cue presentations. For the within-trial pauses ('pause'), the
732 instruction was to further attend to the fixation cross with minimal movement of the fingers or other
733 body parts because these phases served as baseline for the EEG data analysis. Stimulus-response
734 mapping was acquired during a training session held one day prior to the experiment. In this training
735 session, a general familiarization with the keyboard was followed by the standardized frequency
736 adjustment procedure. Subsequently, the visual cues were introduced with a visual presentation after
737 which on average 44±21 minutes (young: 36±16min., older: 51±23min.) of training were performed
738 in the individual tapping frequency until the participants were able to successfully perform one block
739 of 14 trials. In the main experiment, the individual tapping frequency was re-adjusted and the
740 participants performed in total 12 blocks of on average 14 trials each. Each block had a duration of
741 approximately 4 minutes. Participants were given short breaks of individual length between each
742 block in order to rest the eyes and make small movements.

EEG recording and pre-processing

Continuous EEG was recorded from 127 cephalic active surface electrodes (actiCAP, BrainProducts GmbH, Gilching/Germany) arranged according to the 10-10 system and referenced to the FCz electrode (implicit reference). Scalp-electrode impedance was kept below 20kΩ. Data were acquired with a sampling rate of 1kHz (BrainVision Recorder, version 1.21.0004, BrainProducts GmbH, Gilching/Germany).

Electrooculogram (EOG) was recorded using bipolar channels. For the EOG, silver/silver-chloride cup electrodes were placed on the left and right zygomatic processes (horizontal EOG) and on the left supraorbital process as well as on the sphenoid bone below the eye (vertical EOG).

All EEG data (pre-) processing and analyses were performed using functions from the EEGLAB toolbox version 2019.0 [62], the Fieldtrip toolbox version 20190419 [63], and customised Matlab functions (Matlab 2018b, MathWorks, Natick, MA, USA).

Off-line, data from EEG channels were high-pass filtered with a 1Hz cut-off to remove baseline drift and down-sampled to 250Hz. Line noise at 50 and 100Hz was removed based on a frequency-domain (multi-taper) regression with the 'pop_cleanline' function of EEGLAB. Subsequently, continuous data were segmented into epochs of 5 seconds length, ±2.5 seconds around the "start" (baseline) and the "transition" (time of interest) events in order to limit the effect of edge artifacts (Figure 1b).

Thereafter, a rigorous artefact removal pipeline was employed to minimize the effect of high muscle-related artefact while ensuring sufficient data for subsequent analyses. This procedure included a combination of semi-automatic and visual inspection steps. First, bad channels were identified and removed (EEGLAB trimOutlier plugin with 2µV as lower and 100µV as higher cut-off for identification of bad channels). Then canonical correlation analysis (implemented in the EEGLAB AAR plugin) [64] was used to identify and remove excessive EMG activity present in the data due to the motor task (288 seconds window length and shift between correlative analysis windows, 10^6 eigenratio, 15Hz, ratio of 10, based on the welch algorithm). Thereafter, independent component analysis (runica/Infomax algorithm as implemented in EEGLAB) and SASICA was used as a semi-

770 automatic procedure to inform removal of eye-movement -related and residual muscle artefacts [65]. For
771 the identification of ICs representing relevant artifacts, MARA, FASTER, and ADJUST algorithms
772 were used, and components were rejected if they contributed ≥4% of the total data variance. Epochs
773 with remaining muscle artefacts were removed based on trial-by-trial visual inspection. On average 50
774 trials per condition/participant went into further analysis. As a final step, available EEG channels
775 were re-referenced to a common average reference.

776 ## Localization of neuronal sources

777 For the forward solution, an individual head model was created for each participant based on the same
778 high-resolution structural MR image as used for the MRS analysis and 3D locations of the electrodes,
779 registered with an optical infrared-camera based (NDI, Ontario, Canada) neuronavigation system
780 (xensor™, ANT Neuro, Enschede, Netherlands). For the individual geometrical description of the
781 head (mesh), the anatomical image was segmented into 12 tissue classes (skin, eyes, muscle, fat,
782 spongy bone, compact bone, cortical gray matter, cerebellar gray matter, cortical white matter,
783 cerebellar white matter, cerebrospinal fluid and brain stem), based on the MIMA model [66] using
784 SPM12 (http://www.fil.ion.ucl.ac.uk/spm/software/spm12/) as described previously [67–69]. The EEG
785 electrode positions were rigidly co-registered to the individual head surface (skin contour) by
786 projecting the electrode coordinates in the native space through a rigid-body transformation, based on:
787 (i) the estimation of anatomical landmarks (nasion, left/right peri-auricular points), (ii) the alignment
788 of the electrode positions on the head surface through Iterative-Closest Point registration, and (iii) the
789 projection of the electrodes onto the surface choosing the smallest Euclidean distance [70]. Conductivity
790 values for each tissue class were grounded on previous findings [71,72]. Dipole sources were constrained
791 by a regularly spaced 6mm three-dimensional grid spanning both the cortical/subcortical and the
792 cerebellar gray matter. The volume conductor model was constructed based on a whole-head finite
793 element model [73] using the SimBio toolbox (https://www.mrt.uni-jena.de/simbio) implemented in
794 FieldTrip. In order to solve the inverse problem of describing the source activity, we made use of

exact low-resolution brain electromagnetic tomography (eLoreta) algorithm [74], using a regularization factor $\lambda = .05$.

Source space time series were reconstructed using the precomputed filter for three regions of interest, the left and right primary motor cortex and the occipital cortex. Coordinates for these regions of interest were extracted from the group (OLDER vs. YOUNG) averages of the individual centroid coordinates of the MRS voxels in MNI space and transformed into native space. We used a sphere with a 6mm radius around the coordinates as a search grid to retrieve the gray matter grid voxel with the shortest distance to the coordinates of interest. Subsequently, singular value decomposition was used to reduce the dimensionality of the source activity time series in the target voxel from the x-, y- and z-components of the equivalent current dipole source to the projection that carried the maximal signal variance, i.e. the largest (temporal) eigenvector.

Cortico-cortical connectivity

In order to study the connectivity between cortical sources as a function of time, wavelet-based inter-site phase clustering, ISPC [75] was used. This phase-based connectivity measure depends on the distribution of the phase angle differences of two signals in polar space. The underlying assumption is that two neural sources are functionally coupled when their oscillations show temporal synchronization evidenced by angular differences. ISPC is a non-directional measure and has been shown to be less sensitive to time lags, non-stationarity of frequencies, and varying levels of noise [76].

In order to extract the phase angles, spectral decomposition was computed by convolving the ROI source signal with a set of complex Morlet wavelets, defined as complex sine waves tapered by a Gaussian [77]. The frequencies of the wavelets were chosen from 2 Hz to 40 Hz in 50 logarithmically spaced steps in order to retrieve the full theta to beta frequency range. The full-width half-maximum (FWHM) ranged from 400 to 104ms with increasing wavelet peak frequency, corresponding to a spectral FWHM varying between 1.5 Hz and 12 Hz [78]. Subsequently, ISPC was computed for 35 frequency steps from 5:40 Hz.

The phase angle differences were computed between ROI source signals over time and averaged over transition modes [75,79] on the down-sampled data (50Hz) following

Eq.1 $$ISPC_f = \left| n^{-1} \sum_{t=1}^{n} e^{i(\phi_{xt} - \phi_{yt})} \right|$$

where n is the number of time points, and ϕ_x and ϕ_y are phase angles from signals x and y at frequency f. Temporal modulation of ISPC change was evaluated in the time of interest (0 to +2000 post-cue, Figure 1b) relative to the baseline period (-500 to -200ms) computed by subtracting the baseline ISPC values from the ISPC values in the time of interest.

Additionally, instantaneous power was calculated by squaring the complex convolution results. Power spectra were normalized by converting the values to dB change relative to the fused within-trial baseline period, which was generated by averaging the time window between -500 and -200ms before the cue over all start trials [80].

Statistical analysis

The statistical analysis involved in a first step the analysis of the individual outcome modalities (MRS, behavior, and EEG) and in a second step the joined analysis of all three outcome modalities. Generally, for all generalized linear mixed effects models (GLMM) described hereafter, the goodness of fit was visually inspected based on the distribution of residuals. Models were fitted with a random intercept on subject level after validating that this improved model fit compared to the fixed effects model. Model comparison was performed based on Akaike Information Criterion (AIC) and Bayesian Information Criterion (BIC). Parameter estimates for fixed effects and their interactions as well as 95% Confidence Intervals (CIs) and p-values were computed using Wald approximation. Parameter estimates for logistic models are reported as logits, i.e. log odds, as well as odds ratios. In the case of the beta model with logit link, parameter estimates are reported as proportions and change in rate of proportion. Standardized parameters were obtained by fitting the model on a standardized version of the dataset. Relevant interactions were followed up with contrasts for model estimated marginal means of parameter levels and reported as standardized differences (ΔEMM±standard error, 95% CI,

z-value, p-value adjusted for multiple comparisons with Holm's method). Effect sizes are reported for the models' total explanatory power with conditional R^2 and for the fixed effects part alone with marginal R^2 [81] [82]. Forest plots are used to given an overview over the models' parameter estimates with CI, direction, and significance of their effects. Distribution and boxplots are used to represent summary statistics of group data. Computed variables for boxplots: lower/upper whiskers represent smallest/largest observation greater than or equal to lower hinge ± 1.5 * inter- quartile range (IQR), lower/upper hinge reflects 25%/75% quantile, lower edge of notch = median − 1.58 * IQR/ sqrt(n), middle of notch reflects group median.

Analysis of the MRS data

GABA+ data were best estimated with a GLMM showing optimized fit modelling a gamma distribution and identity link function. Factors GROUP, VOXEL, and their interaction were modelled as fixed effects based on the study design variables. Random intercepts were fit on subject level. In order to identify the influence of the quality metrics and raw grey matter fraction (GM fraction) and their potential interaction with group or voxel, a stepwise backwards selection approach was taken starting from a beyond optimal model with all covariates and their interaction with voxel or group. Based on the significance of parameters in the analysis of deviance (Type II Wald statistics), non-significant interactions were eliminated.

Analysis of the behavioral data

Error rate. To analyze the occurrence of errors within the behavioral task, we chose to code and analyze three different aspects of the error information in the data in order to account for the skewed distribution of percentage data and the inherently zero-inflated data.

First, the data was transformed in a binary outcome coding *failed transitions*, i.e. trials with an error rate of 100%. Binarization of the data was achieved by coding fully erroneous trials as "1" and all other trials as "0". This step was done based on the full set of available trials. A GLMM was used as a hurdle model and fit to the data with a Poisson distribution and logit link.

Second, after removing the fully erroneous trials, the remaining data was transformed in a binary outcome coding *fully correct transitions*, i.e. an error rate of 0 coded as "1", versus erroneous trials, i.e. and error rate >0 coded as "0". As described in the first step, a GLMM was used as a hurdle model and fit to the data with a Poisson distribution and logit link.

Third, *cumulative error rate* in the trials not considered fully correct or fully erroneous, i.e. non-zero-inflated trials, were transformed into the range of the beta distribution [0<error rate/100<1] and modelled as such using a GLMM with a "logit" link function. For all three error-rate-based outcomes, factors GROUP (old, young), TRANSITION MODE (into IP, intoAP), and covariate nTRIALc (trial number, centered) were entered into the model as fixed effects including all possible interactions. To account for intra-individual variability, random intercepts were modelled on subject level.

Transition Latency. Transition latency did not follow a normal distribution and was therefore analyzed with a GLMM showing optimized fit assuming a gamma distribution and log link function. In analogy to the models for error rate, factors GROUP (old, young), TRANSITION MODE (into IP, into AP), and covariate nTRIALc (trial number, centered) were modeled as fixed effects including all possible interactions. Random intercepts were modelled on subject level.

The association between transition latency and error rate (excluding failed transitions) was estimated for transition modes within age groups separately using a non-linear locally-weighted smoothing fitted over subgroups.

The additional thumb reaction time task (tRT) was analyzed separately; methods and results are reported Supplementary Note 1 and Supplementary Table 10.

Analysis of the EEG data

EEG data were analyzed with the main focus on phase-related connectivity (ISPC) between motor-cortical source and the signal from intrinsic hand muscles. The statistical analysis of the task-related modulation of the spectral signature followed the pipeline described for ISPC below. Additional methods and results are presented in Supplementary Note 2 and Supplementary Figure 1 to allow the interpretation of the association/independence of ISPC and spectral power changes.

The effect of transition mode and age group on the frequency-band specific modulation of connectivity (inter-site phase clustering, ISPC) was analyzed in three steps. First, ISPC change from baseline was analyzed within subject using a cluster corrected permutation (1000 permutations, 2-tailed t-test, $p<.05$) to extract the effect size of change from baseline irrespective of transition mode. This step was used to extract the z-transformed ISPC changes (zISPC) per condition within subject. In this and the subsequent steps, clusters were corrected for multiple comparisons and considered significant if they contained more time × frequency data points than expected under the null hypothesis at $p<.05$ [83].

Second, group-level cluster-based permutation analysis (1000 permutations, 2-tailed t-test, $p<.05$) of change in baseline-subtracted zISPC pooled over transition modes (stimulus-locked analysis) was used to confirm the relevance of connectivity modulation within the selected time and frequency windows. The results of this second step containing the stimulus-locked analysis of connectivity modulation are presented in Supplementary Figure 2.

Third, in order to test the effect transition mode and its modulation by age group, differences of the z matrices were calculated for the transition mode contrast (IP – AP) for the age groups separately and subsequently subtracted from each other ([IP-AP]YOUNG – [IP-AP]OLDER). A two-sided t-test ($p<.05$) was then run with permuting the age group allocation (1000 permutations).

The third step was performed relative to the response, i.e. ±260ms around the individual median transition latency specific for IP and AP transitions, respectively (response-locked analysis). As task-related connectivity was not modulated by an interaction of condition and age group; therefore, both factors were tested subsequently in separate t-tests permuting the respective factor level allocation (1000 permutations, $p<.05$).

Analysis of the association between phase-angle differences and behavior

Frequency-specific phase angle differences between left and right M1 were extracted for each trial at the respective trial-based time of transition for the low (15-22Hz) and high beta (25-30Hz) frequency ranges identified in the respective time × frequency clusters during the previous analysis step. To rule out randomness of phase angle differences, non-uniformity of their distribution was tested using the

Rayleigh test. A two-way ANOVA for circular data was used to test between-group differences and their interaction with GABA+ concentration. For this analysis step, artificial dichotomization of GABA+ concentration (into below and above within group median concentration) was necessary [84]. Phase angle differences were then correlated with the single trial error rate following the transition using circular-linear correlation. To validate the specificity of the effects in terms of task-context and topography, the same analyses steps were run for two control conditions, namely the LM1-RM1 phase lag at a random time point during baseline [start cue – 300ms], i.e. during between trial pauses (Figure 1b), and for phase angle differences for the OCC-L/RM1 connectivity at the time of transition. All circular statistics and visual representations were performed with CircStat [85] and CircHist (https://github.com/zifredder/CircHist) Toolboxes implemented for Matlab 2018b and R package circular (version 0.4-93) [86]. All results are reported with FDR-corrected [87] p-values (p_{FDR})to account for multiple comparisons across all subgroups.

Analysis of the association between connectivity and behavior through GABA+

The next goal was to get further insight into the relationship between EEG-derived connectivity metrics and behavior and the potential impact of endogenous GABA+ levels on this relationship in the presence of the effect of age. Therefore, we made use of Bayesian moderated mediation analysis modelling GABA+ as mediator and age as moderator variable and their impact on the relationship between cortico-cortical and cortico-spinal connectivity and behavior, i.e. *transition latency* and *error rate* (including *cumulative error rate* and fully *correct transitions* but excluding *failed transitions*). This approach allowed us to further dissect the connectivity – behavior relationship given the individual variations of background GABA+ levels in the context of assumed aging-related changes of the associations between all variables. The Bayesian approach permits accounting for the non-gaussian data structure of the present sample and its size [88]. Conceptually, a moderated mediation model is built based on two regression models, in this case two generalized linear models, one that estimates the effect of the independent variables and relevant covariates (here the moderator) on the dependent variable (the outcome model, Eq. 2), and the second, which estimates the effect of the independent variable and relevant covariates on the mediator (the mediator model, Eq. 3):

Eq. 2 $Y = i_1 + c_1X + c_2W + c_3XW + b_1M + b_2MW + e_1$

Eq. 3 $M = i_2 + a_1X + a_2W + a_3XW + e_2.$

In these models, $i_1$and i_2 are intercepts, Y is the dependent variable, X is the independent variable, M is the mediator, and W is the moderator W interacting with each variable. In the outcome model (Eq. 2), $c1$ is the coefficient relating the independent variable and the dependent variable, b_1 is the coefficient relating the moderator to the dependent variable, c_2 identifies the coefficient relating moderator and independent variable, the coefficients for the interactions with the moderator are c_3 and b_2. In the mediator model (E. 3.), a_1 is the coefficient relating the independent variable with the mediator, a_2 is the coefficient relating the moderator with the mediator, and a_3 is the coefficient for the interaction of the independent variable and the moderator. The residuals are identified by e_1 and e_2. These two models are combined within one multilevel model and estimated simultaneously for the moderated mediation analysis.

Here, a series of individual moderated mediation models was run for left M1- right M1conncectivity, using the respective zISPC pooled over the significant time × frequency clusters in addition to the GABA+ values of the corresponding voxel (e.g. model 1: predictor variable left M1 – right M1 zISPC, outcome variable transition latency, mediator variable left M1 GABA+, model 2: predictor variable left M1 – right M1 zISPC, outcome variable transition latency, mediator variable right M1 GABA+). Coordination pattern (IP vs. AP) was included in the outcome model to account for its significant impact on both behavior and connectivity. Within each moderated mediation model, different associations (model paths) moderated by age were jointly estimated: i) the association between independent and dependent variable in the absence of mediation (path τ, total effect); ii) the association between independent variable and mediator (path α); iii) the association between mediator and dependent variable (path β); iii) the mediation effect (α*β, indirect effect); and iv) the association between independent and dependent variable after adjusting for mediation (path τ', direct effect) [88]. A schematic of the moderated mediation model framework is given in the inlay in Figure 1a on the top right.

All input variables were centered prior to fitting the GLMMs for outcome and mediator models using an exgaussian distribution, identity link functions (for mu, sigma, and beta), and uniform priors. Posterior distributions for multivariate models were obtained using Hamiltonian Monte-Carlo algorithm using Stan [89] implemented for R with brms [90,91] and rstanarm [92] packages. Four random walk chains each with 10.000 iterations discarding the first 1000 iterations (burn-in) were used for inference. Model convergence was examined using pareto-k diagnostics, approximate leave-one-out criterium (LOO), R-hat, and effective sample size (bulk-/tail-ESS); Bayesian R^2 served as indicator for quality of model fit. Median estimates and non-equi-tailed 89% credible intervals, i.e. Highest Density Intervals (89% HDI), are used to describe centrality and quantify uncertainties of the regression coefficients for the individual model paths accounting for their assumed skewness. In order to disentangle the influence of the mediator depending on variations of the moderator, a conditional process analysis was employed. Specifically, conditional estimates were simulated based on posterior draws for lowest versus highest sample quintiles of mediator and moderator. To allow for inferences about the relevance of the effects, probability of direction is reported (pd) for posterior probabilities, which can be interpreted as the probability (expressed in percentage) that a parameter (described by its posterior distribution) is strictly positive or negative. The pd can take values between 50 (one half on each side) and 100 (fully on either side) and is approximated to a frequentist 2-sided p-value with the formula p-value = 2*(1-pd/100) [93,94]. Hence, a pd of 95, 97.5, 99.5, and 99.95% corresponds to p-value at the thresholds 0.1, 0.05, 0.01, 0.001.

Data availability

General source data are not publicly available due to European legal restrictions compromising the research participants' privacy and consent. Source data to reproduce results given in figures 2-7 are provided under [https://figshare.com/s/c2df37a0f7f68b9d208c]. Code to reproduce the results is available from the corresponding author [KFH].

Acknowledgments

We thank René Clerckx for software and technical support and Paul Meugens for technical support and skillful building of the technical equipment, and all volunteers for their motivation to participate.

Funding disclosure

This work was supported by the Internal Research Fund KU Leuven (PDM/15/182) and the Research Foundation Flanders (1509816N, G089818N, G0F7616N, I005018N), the Excellence of Science grant (EOS, 30446199, MEMODYN), the KU Leuven Research Fund (C16/15/070), and Science Foundation Ireland (18/IF/6272).

Competing Interests

The authors declare that no competing interests exist.

References

1. Steyvers, M., Hawkins, G. E., Karayanidis, F. & Brown, S. D. A large-scale analysis of task switching practice effects across the lifespan. *Proceedings of the National Academy of Sciences* **116**, 17735-17740 (2019).
2. Rozycka, A. & Liguz-Lecznar, M. The space where aging acts: focus on the GABAergic synapse. *Aging Cell* **16**, 634-643 (2017).
3. Buzsáki, G., Geisler, C., Henze, D. A. & Wang, X. J. Interneuron Diversity series: Circuit complexity and axon wiring economy of cortical interneurons. *Trends Neurosci* **27**, 186-193 (2004).
4. McBain, C. J. & Fisahn, A. Interneurons unbound. *Nat Rev Neurosci* **2**, 11-23 (2001).
5. Cardin, J. A. Inhibitory interneurons regulate temporal precision and correlations in cortical circuits. *Trends in neurosciences* **41**, 689-700 (2018).
6. Fries, P. A mechanism for cognitive dynamics: neuronal communication through neuronal coherence. *Trends in cognitive sciences* **9**, 474-480 (2005).
7. Fries, P. Rhythms for cognition: communication through coherence. *Neuron* **88**, 220-235 (2015).
8. Heise, K. F. et al. The aging motor system as a model for plastic changes of GABA-mediated intracortical inhibition and their behavioral relevance. *J Neurosci* **33**, 9039-9049 (2013).
9. Hermans, L. et al. Age-related alterations in the modulation of intracortical inhibition during stopping of actions. *Aging (Albany NY)* **11**, 371-385 (2019).

10. Spooner, R. K., Wiesman, A. I., Proskovec, A. L., Heinrichs-Graham, E. & Wilson, T. W. Rhythmic Spontaneous Activity Mediates the Age-Related Decline in Somatosensory Function. *Cereb Cortex* **29**, 680-688 (2019).
11. Marenco, S. et al. Role of gamma-amino-butyric acid in the dorsal anterior cingulate in age-associated changes in cognition. *Neuropsychopharmacology* **43**, 2285-2291 (2018).
12. Cassady, K. et al. Sensorimotor network segregation declines with age and is linked to GABA and to sensorimotor performance. *Neuroimage* **186**, 234-244 (2019).
13. Houweling, S., Beek, P. J. & Daffertshofer, A. Spectral changes of interhemispheric crosstalk during movement instabilities. *Cereb Cortex* **20**, 2605-2613 (2010).
14. Coxon, J. P. et al. Reduced basal ganglia function when elderly switch between coordinated movement patterns. *Cereb Cortex* **20**, 2368-2379 (2010).
15. Mikkelsen, M. et al. Big GABA: Edited MR spectroscopy at 24 research sites. *Neuroimage* **159**, 32-45 (2017).
16. Hermans, L. et al. GABA levels and measures of intracortical and interhemispheric excitability in healthy young and older adults: an MRS-TMS study. *Neurobiology of Aging* **65**, 168-177 (2018).
17. Maes, C. et al. Age-related differences in GABA levels are driven by bulk tissue changes. *Hum Brain Mapp* **39**, 3652-3662 (2018).
18. Meyer-Lindenberg, A., Ziemann, U., Hajak, G., Cohen, L. & Berman, K. F. Transitions between dynamical states of differing stability in the human brain. *Proc Natl Acad Sci U S A* **99**, 10948-10953 (2002).
19. Aramaki, Y., Haruno, M., Osu, R. & Sadato, N. Movement initiation-locked activity of the anterior putamen predicts future movement instability in periodic bimanual movement. *J Neurosci* **31**, 9819-9823 (2011).
20. Banerjee, A., Tognoli, E., Kelso, J. A. & Jirsa, V. K. Spatiotemporal re-organization of large-scale neural assemblies underlies bimanual coordination. *Neuroimage* **62**, 1582-1592 (2012).
21. Heise, K. F., Monteiro, T. S., Leunissen, I., Mantini, D. & Swinnen, S. P. Distinct online and offline effects of alpha and beta transcranial alternating current stimulation (tACS) on continuous bimanual performance and task-set switching. *Sci Rep* **9**, 3144 (2019).
22. Palva, J. M. et al. Ghost interactions in MEG/EEG source space: A note of caution on inter-areal coupling measures. *Neuroimage* **173**, 632-643 (2018).
23. Nikouline, V. V., Linkenkaer-Hansen, K., Huttunen, J. & Ilmoniemi, R. J. Interhemispheric phase synchrony and amplitude correlation of spontaneous beta oscillations in human subjects: a magnetoencephalographic study. *Neuroreport* **12**, 2487-2491 (2001).
24. O'Reilly, C. & Elsabbagh, M. Intracranial recordings reveal ubiquitous in-phase and in-antiphase functional connectivity between homotopic brain regions in humans. *J Neurosci Res* **99**, 887-897 (2021).
25. Cuypers, K. et al. Task-related measures of short-interval intracortical inhibition and GABA levels in healthy young and older adults: A multimodal TMS-MRS study. *Neuroimage* **208**, 116470 (2019).
26. Maes, C. et al. GABA levels are differentially associated with bimanual motor performance in older as compared to young adults. *NeuroImage* 117871 (2021).
27. Ilic, T. Subtle hemispheric asymmetry of motor cortical inhibitory tone. *Clinical Neurophysiology* **115**, 330-340 (2004).
28. Shin, H.-W., Sohn, Y. H. & Hallett, M. Hemispheric asymmetry of surround inhibition in the human motor system. *Clinical Neurophysiology* **120**, 816-819 (2009).
29. Vallence, A.-M., Smalley, E., Drummond, P. D. & Hammond, G. R. Long-interval intracortical inhibition is asymmetric in young but not older adults. *Journal of Neurophysiology* **118**, 1581-1590 (2017).
30. Stagg, C. J. et al. Relationship between physiological measures of excitability and levels of glutamate and GABA in the human motor cortex. *J Physiol* **589**, 5845-5855 (2011).
31. Dyke, K. et al. Comparing GABA-dependent physiological measures of inhibition with proton magnetic resonance spectroscopy measurement of GABA using ultra-high-field MRI. *Neuroimage* **152**, 360-370 (2017).

32. Hoshino, O., Kameno, R. & Watanabe, K. Reducing variability in motor cortex activity at a resting state by extracellular GABA for reliable perceptual decision-making. *J Comput Neurosci* **47**, 191-204 (2019).
33. Farrant, M. & Nusser, Z. Variations on an inhibitory theme: phasic and tonic activation of GABA(A) receptors. *Nat Rev Neurosci* **6**, 215-229 (2005).
34. Restuccia, D. et al. Contribution of GABAergic cortical circuitry in shaping somatosensory evoked scalp responses: specific changes after single-dose administration of tiagabine. *Clin Neurophysiol* **113**, 656-671 (2002).
35. Muthukumaraswamy, S. D. et al. Elevating endogenous GABA levels with GAT-1 blockade modulates evoked but not induced responses in human visual cortex. *Neuropsychopharmacology* **38**, 1105-1112 (2013).
36. Buffalo, E. A., Fries, P., Landman, R., Buschman, T. J. & Desimone, R. Laminar differences in gamma and alpha coherence in the ventral stream. *Proc Natl Acad Sci U S A* **108**, 11262-11267 (2011).
37. Traub, R. D. et al. Layer 4 pyramidal neuron dendritic bursting underlies a post-stimulus visual cortical alpha rhythm. *Commun Biol* **3**, 230 (2020).
38. Adams, N. E. et al. GABA-ergic Dynamics in Human Frontotemporal Networks Confirmed by Pharmaco-Magnetoencephalography. *J Neurosci* **40**, 1640-1649 (2020).
39. Leventhal, A. G. GABA and Its Agonists Improved Visual Cortical Function in Senescent Monkeys. *Science* **300**, 812-815 (2003).
40. Schmolesky, M. T., Wang, Y., Pu, M. & Leventhal, A. G. Degradation of stimulus selectivity of visual cortical cells in senescent rhesus monkeys. *Nat Neurosci* **3**, 384-390 (2000).
41. Hall, S. D. et al. The role of GABAergic modulation in motor function related neuronal network activity. *Neuroimage* **56**, 1506-1510 (2011).
42. Hoshino, O., Zheng, M. & Watanabe, K. Reduction of trial-to-trial perceptual variability by intracortical tonic inhibition. *Neural computation* **28**, 187-215 (2016).
43. Lalwani, P. et al. Neural distinctiveness declines with age in auditory cortex and is associated with auditory GABA levels. *Neuroimage* **201**, 116033 (2019).
44. Goh, J. O. Functional Dedifferentiation and Altered Connectivity in Older Adults: Neural Accounts of Cognitive Aging. *Aging Dis* **2**, 30-48 (2011).
45. Damoiseaux, J. S. Effects of aging on functional and structural brain connectivity. *NeuroImage* **160**, 32-40 (2017).
46. King, B. R. et al. Age-Related Declines in Motor Performance are Associated With Decreased Segregation of Large-Scale Resting State Brain Networks. *Cereb Cortex* **28**, 4390-4402 (2018).
47. Moezzi, B. et al. Characterization of Young and Old Adult Brains: An EEG Functional Connectivity Analysis. *Neuroscience* **422**, 230-239 (2019).
48. Wang, B. et al. Increased Functional Brain Network Efficiency During Audiovisual Temporal Asynchrony Integration Task in Aging. *Front Aging Neurosci* **10**, 316 (2018).
49. Michely, J. et al. Network connectivity of motor control in the ageing brain. *Neuroimage Clin* **18**, 443-455 (2018).
50. Oldfield, R. C. The assessment and analysis of handedness: The Edinburgh inventory. *Neuropsychologia* **9**, 97-113 (1971).
51. Peek, A. L. et al. Brain GABA and glutamate levels across pain conditions: A systematic literature review and meta-analysis of 1H-MRS studies using the MRS-Q quality assessment tool. *NeuroImage* **210**, 116532 (2020).
52. Yousry, T. A. et al. Localization of the motor hand area to a knob on the precentral gyrus. A new landmark. *Brain* **120**, 141-157 (1997).
53. Baumgarten, T. J. et al. Beta Peak Frequencies at Rest Correlate with Endogenous GABA+/Cr Concentrations in Sensorimotor Cortex Areas. *PLoS One* **11**, e0156829 (2016).
54. Mescher, M., Merkle, H., Kirsch, J., Garwood, M. & Gruetter, R. Simultaneous in vivo spectral editing and water suppression. *NMR in Biomedicine: An International Journal Devoted to the Development and Application of Magnetic Resonance In Vivo* **11**, 266-272 (1998).

55. Edden, R. A., Puts, N. A., Harris, A. D., Barker, P. B. & Evans, C. J. Gannet: A batch-processing tool for the quantitative analysis of gamma-aminobutyric acid–edited MR spectroscopy spectra. *J Magn Reson Imaging* **40**, 1445-1452 (2014).
56. Near, J. et al. Frequency and phase drift correction of magnetic resonance spectroscopy data by spectral registration in the time domain. *Magn Reson Med* **73**, 44-50 (2015).
57. Mikkelsen, M. et al. Big GABA II: Water-referenced edited MR spectroscopy at 25 research sites. *Neuroimage* **191**, 537-548 (2019).
58. Rothman, D. L., Petroff, O. A., Behar, K. L. & Mattson, R. H. Localized 1H NMR measurements of gamma-aminobutyric acid in human brain in vivo. *Proc Natl Acad Sci U S A* **90**, 5662-5666 (1993).
59. Edden, R. A. E., Puts, N. A. J. & Barker, P. B. Macromolecule-suppressed GABA-edited magnetic resonance spectroscopy at 3T. *Magnetic resonance in medicine* **68**, 657-661 (2012).
60. Harris, A. D., Puts, N. A. J. & Edden, R. A. E. Tissue correction for GABA-edited MRS: Considerations of voxel composition, tissue segmentation, and tissue relaxations. *Journal of Magnetic Resonance Imaging* **42**, 1431-1440 (2015).
61. Schöner, G. & Kelso, J. A. Dynamic pattern generation in behavioral and neural systems. *Science* **239**, 1513-1520 (1988).
62. Delorme, A. & Makeig, S. EEGLAB: an open source toolbox for analysis of single-trial EEG dynamics including independent component analysis. *J Neurosci Methods* **134**, 9-21 (2004).
63. Oostenveld, R., Fries, P., Maris, E. & Schoffelen, J. M. FieldTrip: Open source software for advanced analysis of MEG, EEG, and invasive electrophysiological data. *Comput Intell Neurosci* **2011**, 156869 (2011).
64. Gomez-Herrero, G. et al. Automatic Removal of Ocular Artifacts in the EEG without an EOG Reference Channel. *Proceedings of the 7th Nordic Signal Processing Symposium - NORSIG 2006* (2006).
65. Chaumon, M., Bishop, D. V. M. & Busch, N. A. A practical guide to the selection of independent components of the electroencephalogram for artifact correction. *Journal of Neuroscience Methods* **250**, 47-63 (2015).
66. Iacono, M. I. et al. MIDA: A Multimodal Imaging-Based Detailed Anatomical Model of the Human Head and Neck. *PLOS ONE* **10**, e0124126 (2015).
67. Samogin, J., Liu, Q., Marino, M., Wenderoth, N. & Mantini, D. Shared and connection-specific intrinsic interactions in the default mode network. *NeuroImage* **200**, 474-481 (2019).
68. Liu, Q., Ganzetti, M., Wenderoth, N. & Mantini, D. Detecting Large-Scale Brain Networks Using EEG: Impact of Electrode Density, Head Modeling and Source Localization. *Front Neuroinform* **12**, 4 (2018).
69. Liu, Q., Farahibozorg, S., Porcaro, C., Wenderoth, N. & Mantini, D. Detecting large-scale networks in the human brain using high-density electroencephalography. *Hum Brain Mapp* **38**, 4631-4643 (2017).
70. Taberna, G. A., Marino, M., Ganzetti, M. & Mantini, D. Spatial localization of EEG electrodes using 3D scanning. *J Neural Eng* **16**, 026020 (2019).
71. Haueisen, J., Ramon, C., Eiselt, M., Brauer, H. & Nowak, H. Influence of tissue resistivities on neuromagnetic fields and electric potentials studied with a finite element model of the head. *IEEE Transactions on Biomedical Engineering* **44**, 727-735 (1997).
72. Vorwerk, J., Aydin, U., Wolters, C. H. & Butson, C. R. Influence of Head Tissue Conductivity Uncertainties on EEG Dipole Reconstruction. *frontiers in Neuroscience* **13**, 531 (2019).
73. Wolters, C. H., Grasedyck, L. & Hackbusch, W. Efficient computation of lead field bases and influence matrix for the FEM-based EEG and MEG inverse problem. *Inverse Problems* **20**, 1099-1116 (2004).
74. Pascual-Marqui, R. D. Discrete, 3D distributed, linear imaging methods of electric neuronal activity. Part 1: exact, zero error localization. *arXiv preprint arXiv:0710.3341* (2007).
75. Lachaux, J.-P. et al. Studying single-trials of phase synchronous activity in the brain. *International Journal of Bifurcation and Chaos* **10**, 2429-2439 (2000).
76. Cohen, M. X. Effects of time lag and frequency matching on phase-based connectivity. *Journal of Neuroscience Methods* **250**, 137-146 (2015).

77. Tallon-Baudry & Bertrand. Oscillatory gamma activity in humans and its role in object representation. *Trends Cogn Sci* **3**, 151-162 (1999).
78. Cohen, M. X. A better way to define and describe Morlet wavelets for time-frequency analysis. *Neuroimage* **199**, 81-86 (2019).
79. Mormann, F., Lehnertz, K., David, P. & E. Elger, C. Mean phase coherence as a measure for phase synchronization and its application to the EEG of epilepsy patients. *Physica D: Nonlinear Phenomena* **144**, 358-369 (2000).
80. Ciuparu, A. & Mureşan, R. C. Sources of bias in single-trial normalization procedures. *Eur J Neurosci* **43**, 861-869 (2016).
81. Funder, D. C. & Ozer, D. J. Evaluating effect size in psychological research: Sense and nonsense. *Advances in Methods and Practices in Psychological Science* **2**, 156-168 (2019).
82. Chen, H., Cohen, P. & Chen, S. How big is a big odds ratio? Interpreting the magnitudes of odds ratios in epidemiological studies. *Communications in Statistics—simulation and Computation®* **39**, 860-864 (2010).
83. Maris, E. & Oostenveld, R. Nonparametric statistical testing of EEG- and MEG-data. *Journal of Neuroscience Methods* **164**, 177-190 (2007).
84. Harrison, D. & Kanji, G. K. The development of analysis of variance for circular data. *Journal of Applied Statistics* **15**, 197-223 (1988).
85. Berens, P. CircStat: a MATLAB toolbox for circular statistics. *J Stat Softw* (2009).
86. Agostinelli, C. & Lund, U. R package 'circular': Circular Statistics (version 0.4-93). *URL https://r-forge. r-project. org/projects/circular* (2013).
87. Benjamini, Y. & Yekutieli, D. The control of the false discovery rate in multiple testing under dependency. *Annals of statistics* (2001).
88. Yuan, Y. & MacKinnon, D. P. Bayesian mediation analysis. *Psychol Methods* **14**, 301-322 (2009).
89. Carpenter, B. et al. Stan: A Probabilistic Programming Language. *Journal of Statistical Software* **76**, (2017).
90. Bürkner, P.-C. brms: An R Package for Bayesian Multilevel Models Using Stan. *Journal of Statistical Software* **80**, 1-28 (2017).
91. Bürkner, P.-C. Advanced Bayesian Multilevel Modeling with the R Package brms. *The R Journal* **10**, 395 (2018).
92. Goodrich B, G. J., Ali I & Brilleman S. rstanarm: Bayesian applied regression modeling via Stan. R package version 2.19.3. (2020).
93. Makowski, D., Ben-Shachar, M. & Lüdecke, D. bayestestR: Describing Effects and their Uncertainty, Existence and Significance within the Bayesian Framework. *Journal of Open Source Software* **4**, 1541 (2019).
94. Makowski, D., Ben-Shachar, M. S., Chen, S. H. A. & Lüdecke, D. Indices of Effect Existence and Significance in the Bayesian Framework. *Front Psychol* **10**, 2767 (2019).